A LOW-COST AND FLEXIBLE PLATFORM FOR GLOBAL ASSET MONITORING

A Dissertation
Presented to
The Academic Faculty

by

Eric Jonathan Myers

In Partial Fulfillment
of the Requirements for the Degree
Master of Science in the
School of Electrical and Computer Engineering

Georgia Institute of Technology
August 2018

A LOW-COST AND FLEXIBLE PLATFORM FOR GLOBAL ASSET MONITORING

Approved by:

Dr. Deepakraj M. Divan, Advisor
School of Electrical and Computer Engineering
Georgia Institute of Technology

Dr. Raheem A. Beyah
School of Electrical and Computer Engineering
Georgia Institute of Technology

Dr. Gregory D. Durgin
School of Electrical and Computer Engineering
Georgia Institute of Technology

Date Approved: 7/26/2018

Any sufficiently advanced technology

is indistinguishable from magic

Arthur C. Clarke's Third Law

ACKNOWLEDGEMENTS

This thesis would not have been possible without the mentoring and guidance of Dr. Divan. I would like to thank you, as well as Dr. Beyah and Dr. Durgin for your help and feedback while writing this thesis. I appreciate that you took the time and effort to look over my research. I know that as professors, these are two of the most precious resources available.

I would like to thank my parents for their continued support throughout my academic career, my decision to go back to school to pursue a graduate degree, and their reluctant understanding that I will not be attending commencement or buying graduation robes. You have always encouraged me to pursue my interests and have fostered a well-rounded foundation which I have built myself upon. I would like to thank you with words rather than monetarily, as paying you back is highly unlikely.

I would like to thank the Center for Distributed Energy, without your help and funding I would have likely gone into massive debt and am eternally grateful that I didn't. I would like to thank everyone at the CDE and the entirety of team GAMMA. You've made the last two years of work an enjoyable and disconcertingly fast experience. I would like to personally thank Mickaël, Rohit, Kavya, and Yunkyung. While I never worked directly with you, I could always count on you making my day better.

Lastly, I would like to thank coffee, tea, and espresso. Thank you for getting me up in the morning and carrying me on past lunch. Without your imbued magic, I am highly doubtful I would have been half as productive as I should have been.

I could have done without the caffeine headaches though.

TABLE OF CONTENTS

LIST OF TABLES

LIST OF FIGURES

LIST OF ABBREVIATIONS

Abbreviation	Description
ADC	Analog to digital converter
AES	Advanced Encryption Standard
AFE	Analog Front End
BER	Bit Error Rate
BLE	Bluetooth Low Energy
DTN	Delay Tolerant Network
DUT	Device Under Test
GAMMA	Global Asset Monitoring, Management & Analytics
GPIO	General-Purpose Input/output
GPRS	General Packet Radio Service
GSM	Global System for Mobile communication
HMAC	Hashed Message Authentication Code
I2C	Inter-Integrated Circuit
IFA	Inverted F-Antenna
LDO	Low Drop Out
LGA	Landing Grid Array
LNA	Low Noise Amplifier
MCU	Micro Controller
NFC	Near Field Communication

Abbreviation	Description
NIC	Network Interface Card
ODR	On Demand Radio
OSI	Open System Interconnection
PA	Power Amplifier
PCB	Printed Circuit Board
PGA	Programmable Gain Amplifier
RFID	Radio Frequency Identification
RSSI	Received Signal Strength Indicator
RTU	Remote Terminal Unit
SMPS	Switched Mode Power Supply
SPI	Serial Peripheral Interface Bus
UART	Universal Asynchronous Receiver-transmitter
VVO	Volt/VAR Optimization
WDT	Watch Dog Timer

SUMMARY

Conventional approaches to asset monitoring involve high-priced sensors paired with a dedicated radio. These implementations work well when dealing with high-valued property but are not economically viable when the value of the asset approaches the cost of monitoring. Alternative low-cost connectivity solutions, such as IoT, assume the presence of an internet access point which may not be a given for remote locations. These solutions cannot accommodate locations with sparse connectivity and low-cost assets; thus, creating a communication gap.

The research proposed suggests the implementation of a low-cost and intelligent sensor ecosystem which utilizes a Bluetooth based delay-tolerant network. The network functions by leveraging the hardware and internet access of smart devices to bridge the gap between the cloud and devices without internet connection. The hardware for Bluetooth is low-cost and energy efficient, which is crucial for applications that would not otherwise be economically viable.

By consolidating core aspects of the platform technology into a compact and flexible module, new and preexisting designs can readily incorporate delay tolerant network into their systems. Only specific application-based circuitry needs to be implemented externally, which can offload the burden of complex or sensitive design. These provisions can dramatically reduce development time and cost. The network can be made more robust, by incorporating secondary network structures, such as GSM, to work in tandem granting communication flexibility.

CHAPTER 1

INTRODUCTION

The power grid is often touted as the largest and most complex man-made machine. It has become so ubiquitous and encompassing that for many it is more of a fact-of-life than an intricate system that is ever expanding. As the grid grows to accommodate increasing demand and modern technologies, so too do the challenges it faces. With the advent and increasing penetration of intermittent renewable energy sources, the grid is forced to move from a unidirectional, centralized, and deterministic system to a bidirectional, decentralized, and stochastic system [1]. The operation and control of such a system requires intimate knowledge and visibility of the individual nodes [2]. However, the utility grid is largely without intelligent sensing solutions; 60-80% of the more valuable assets used in generation and transmission are monitored, however, only 20% of this data is utilized [3]. Lower valued assets in sub-transmission and distribution systems are rarely monitored.

It is therefore desirable, and in several cases imperative, to make the grid smarter by implementing intelligent and distributed sensor networks to monitor energy devices. These distributed assets present their own unique challenges in terms of reliability, cost, control, communications, and security.

1.1 Background

To make the grid smarter, utilities have introduced initiatives such as large transformer monitoring, PMUs at substations, and AMI deployment at commercial sites

[4]. These measurements encapsulate what is happening on the extremities of the grid, but often overlook distribution level impacts. Efforts made by companies to offer service transformer sensing solutions that can detail voltage, current, harmonics etc., have not been successful as these solutions have not been economically viable. A sensor solution which costs $500-1500 presents very little added value when used to monitor a transformer asset which costs $1250. After factoring in the expected life-time of the sensor (5-10 years), it becomes clear that it is more cost effective to not monitor the asset at all and simply replace it as needed.

Traditional communication structures also present a barrier of entry [5]. These options frequently rely on expensive on-demand-radios (ODR), which require a significant amount of local computation, utilize standards which will be outdated in a few years, and are often geographically limited by the RF bands that they occupy [6]. The wide range of communication options (Fig. 1.1) make it difficult to offer standard and global solutions for what is intended to be a low-cost and ubiquitous network [7]. Many of these entail resources that are oversized for the computation and communication necessary for functionality. Most smart grid applications have bandwidth requirements in the kbps range but might be paying for bandwidth several orders of magnitude higher [6]. The conventional solution of centralized control, and on-demand communication have increased expenditures to untenable levels, while not addressing issues with resiliency, security, or management. Given these challenges, it is not surprising that many asset owners have chosen to completely forgo low-valued asset monitoring all-together.

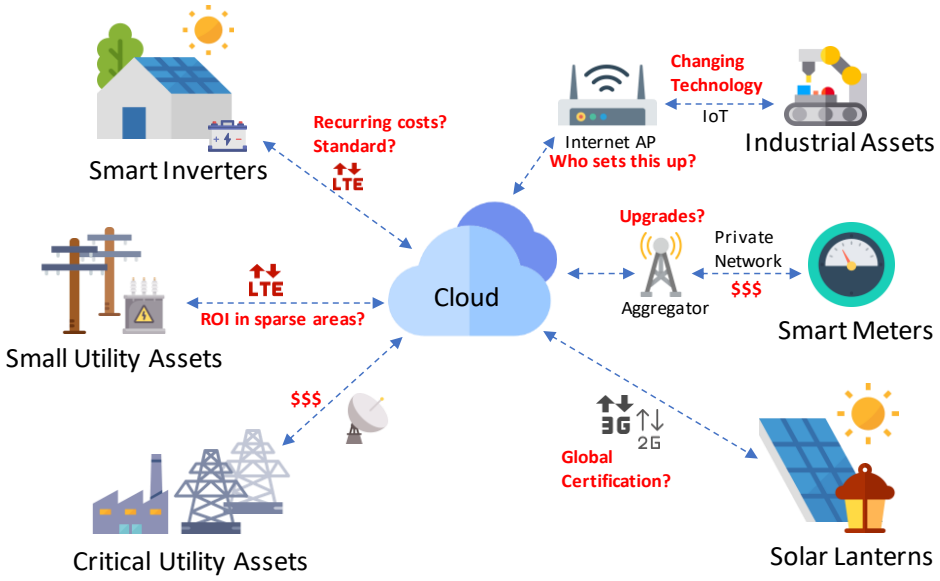

Fig. 1.1: Connectivity issues and economic drawbacks in conventional communication systems.

There has been a concerted effort recently to move monitoring applications to lower cost solutions like Internet-of-Things (IoT), which are rapidly being adopted in smart grids [8]. While options in this space are decidedly cheaper than those with ODR, they still suffer from similar setbacks. IoT solutions depend on pre-defined access points that require constant maintenance and upkeep. Access points can take the form of Wi-Fi routers, or central hub solutions for RF mesh technologies such as Zigbee, Z-Wave, or Long Range Wide Area Network (LoRAWN) [9]. Implementation of these technologies can require customized set-up, and a dedicated pathway to connect end-devices to the cloud. This dedicated path is usually in the form of some recurring cost via a subscription or contract. These solutions still present a disparity in the value of the device to be monitored, and the cost of monitoring which can greatly limit the return on investment (ROI).

1.2 Motivation

If asset owners chose to proceed with monitoring, despite poor ROI, the issue then becomes one of information management. The deluge of raw data generated from the end-devices is only useful if meaningful information and trends are extracted through analytics. Storage and analysis of this nature necessitates an intricate cloud infrastructure with back-end processing, which will only further decrease potential ROI. Maintaining such a framework is further predicated on resources necessary for updates, tech migration, and addressing the perpetual and evolving threat of cyber-attacks. For many low-volume applications, this is simply infeasible.

There is a strong need for a fully integrated platform which is low-cost, flexible, globally compliant, cybersecure, offers cloud-based analytics, and addresses the connectivity gap present in sensor networks. There are promising concepts that are emerging from the IoT ecosystem which look to address these issues. Mobile Crowd Sensing (MCS) can aid in data collection using mobile sensing devices such as smart-phones [10]. Networks with higher latencies have also been proposed in applications with sparse or unreliable connectivity [11] [12] [13]. This research aims to take these concepts further by developing an end-to-end, secure, device-to-cloud platform which relies on smart phones to bridge the communication gap for distributed asset monitoring.

CHAPTER 2

COMMUNICATIONS PLATFORM

To address the communication gap between energy devices and the cloud, this research proposes the implementation of a novel and flexible platform. This chapter details the structure of the network platform, the analytical value it can provide, how it can be protected against cyber threats, and how it can be combined with traditional networks to become more robust.

2.1 GAMMA Platform Overview

The Global Asset Monitoring, Management and Analytics Platform (GAMMA) is a low-cost and intelligent sensor ecosystem which primarily utilizes a Bluetooth based delay-tolerant network (DTN). In lieu of a dedicated communication channel, the DTN leverages the availability and connectivity of smart phones to bridge the communication gap between the energy devices and the cloud.

Several wireless standards and technologies were considered while designing the network architecture. These included Wi-Fi Direct (previously Wi-Fi P2P), ZigBee, RFID, NFC, and others. Many of these posed the problems of not being widely adopted or needing additional and costly hardware to implement. Bluetooth, however, presented several advantages and desirable qualities.

Bluetooth is a widely adopted protocol that is present on every contemporary smart device [14], and thanks to the built in backwards compatibility with previous iterations, presents an extremely minimal risk to tech migration [15]. Bluetooth is also a global

standard and is not geographically locked like GSM bands or GPRS. The hardware necessary for a Bluetooth based network is low cost and requires only a single global certification. Since Bluetooth is a localized and public standard, there are also no recurring costs associated with communication subscriptions or licensing. With the introduction of Bluetooth Low Energy (BLE), the protocol has become energy and computationally efficient; though data throughput has decreased to compensate. Bluetooth also allows for the implementation of custom encryption on the packet level, as well as utilizing the 128-bit Advanced Encryption Standard (AES) which is built into the protocol. When these numerous factors are compared against popular technologies in the same space, the true value of platform beings to stand out (Table 2.1).

Table 2.1: Comparison of GAMMA with popular technologies

	Public ODR	Private ODR	IoT	RFID	GAMMA
Infrastructure cost / unit	Low	High	Moderate	Low	Low
Security	Unsecure	Secure	Secure	Unsecure	Secure
Tech migration	In-Field Upgrade	High Risk	Low Risk	Low Risk	Low Risk
Geographic constraints	Country	Network	Local	Local	Global
In-country certification	Required	Required	Required	Not Required	Not Required
Energy Requirement	High	High	Low	Low	Low
Computation	High	High	High	Low	Low
On-Demand Connect	Available	Available	Available	Unavailable	Optional at Cost
Autonomous Control	Possible	Possible	Possible	Not Possible	Possible
Recurring Costs	Moderate	High	Low	None	None

2.2 Delay Tolerant Network

The DTN works by storing a backlog of data waiting to be transmitted from the asset to the cloud, or from the cloud back to the asset. In the presence of a verified user, the cloud-connected device connects to the asset and can relay information between the asset and the cloud. Since the user is acting as a relay, the asset is completely agnostic to the communication interface to the cloud (3G, LTE, Wi-Fi etc.) This provides a

standardized backbone to connect a multitude of energy devices to the cloud. For assets that require more attention, or have time-sensitive data, the sensor can also be fitted with a dedicated radio as a fall back (Fig. 2.1).

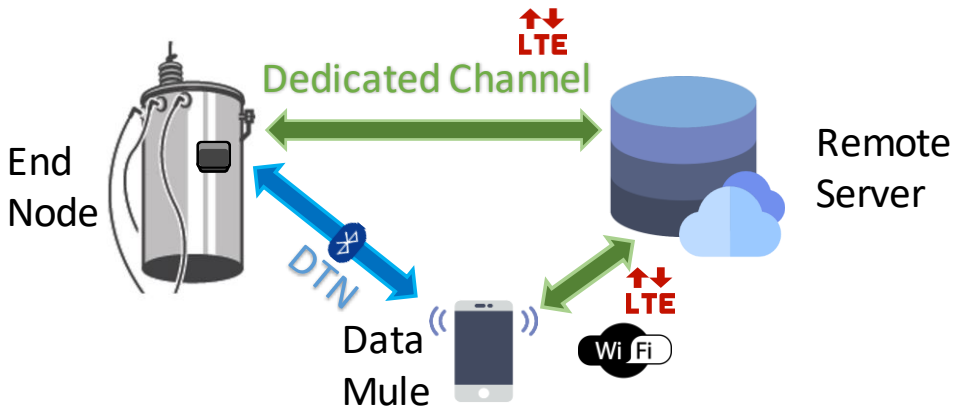

Fig. 2.1: Flexible communication networks allow for multiple paths to the cloud.

2.2.1 End-nodes

The end-node is a GAMMA enabled device which will directly interface with an asset that the user would like to monitor or control. If the end-node does not have a dedicated connection to the internet, it will be entirely dependent on the delay-tolerant network. The delay between connection events can range anywhere from seconds to months, depending on the availability and frequency of exposure to data-mules. Thus, it is required that the end-device be capable of storing several months of data locally in non-volatile memory to prevent data loss or buffering issues.

The end-node will advertise itself as a BLE peripheral device. The frequency of advertisement events will be contingent on the device's power budget and likelihood of encountering a mule. If for instance the end-node is powered on a low capacity coin-cell

battery and is in a remote location, advertising frequently would not be advisable. However, if the device has a constant and reliable source of energy and is likely to encounter a mule, advertising frequently might be innocuous to the system.

On initial set-up via the commissioning process, various system parameters are established on both the end device and the remote server. This includes syncing the real time clock on the end-node and establishing the GPS location of the device on the server. Other parameters might include what kind of devices are being interfaced and monitored with the end-node.

2.2.2 Data-mules

Data-mules serve as the communication bridge between the end-node (data source), and the server (data repository). Data-mules therefore require both Bluetooth and internet connectivity. Any device with the capability of these two technologies is a potential data-mule. However, for most of our considerations data-mules will likely be smart phones, as they possess several advantages. Most phones currently in use are smart phones. These are often equipped with multiple communication topologies such as Wi-Fi, cellular networks, Bluetooth, and near field communication (NFC). Even the most basic and older models have Bluetooth and some form of internet access. Most phones have GPS capabilities, which can be relayed back to the server for geographical analytics and inventory management. Most people also carry their phones on them at all times. For densely populated areas, this means readily available and dependable access to the internet; provided there are enough registered users on the network. All these benefits and features make smart phones the ideal candidate for data-mules. The GAMMA connectivity app can

run in the background and passively connect to local devices without the need of user interaction.

2.2.3 Remote Server

The remote server is responsible for coordinating and managing the end-nodes and data-mules within the network. It will keep records of device locations, last time synced, and other device specific information that is relevant to each use-case. The incoming information from the data-mules will need to be cleansed and analyzed against current records to detect duplicate data and report event as they occur. The server will also push information back to the data-mules, such as the location nearby end-nodes, specific data queries, and information necessary to gain access permission. The information exchanged between the server, the mule application, and the end-node is detailed in Fig. 2.2.

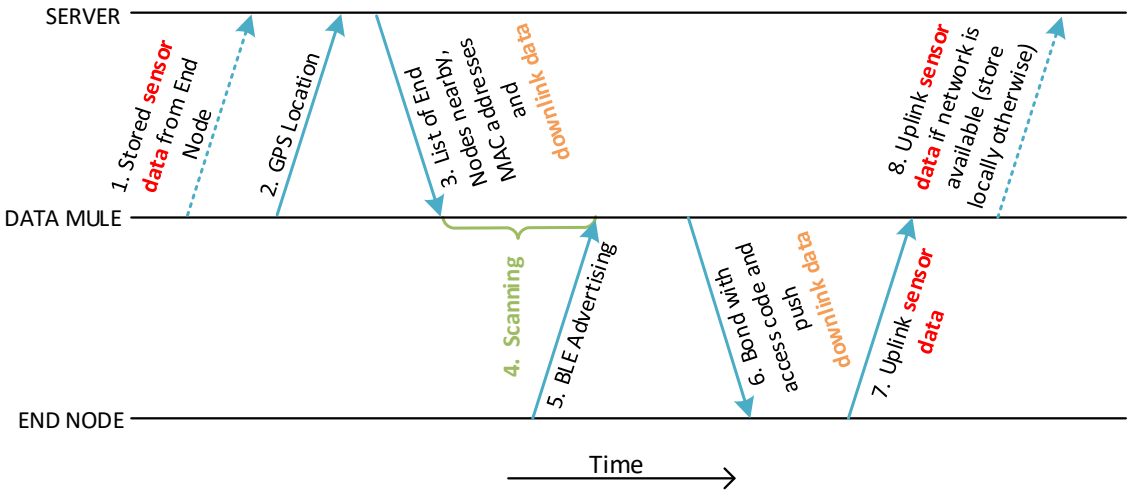

Fig. 2.2: Communication timing diagram.[1]

[1] Diagram content is credited to Qinchen Gu, PhD student at Georgia Institute of Technology and member of GAMMA development team.

From an OSI perspective, the network structure is analogous to a traditional computer network. The end-node and remote server are the end points of an application layer communication channel which will exchange sensor data and downlink data. The data-mule will operate on the network layer and will serve as a direct link routing packets between the two end points. Once the packets have been transferred from the end-node to the data-mule, mature protocols such as TCP and HTTP can handle the transfer from the data-mule to the cloud.

2.2.4 Assumptions and Constraints

Since there are a wide variety of possible end-nodes and data-mules, the network was designed with a few assumptions and constraints:

- The end-node typically does not have direct access to the internet, (e.g., ethernet, Wi-Fi, cellular etc.) It must rely on BLE and a data-mule to connect to the cloud.
- The end-node will be low-cost and low energy. It will either be powered directly from the energy device that it is monitoring or will be able to source locally from a storage device such as a battery. It will be able to remain powered during an asset power outage. This could range from a contingency of a few minutes to days, as is needed by the application.
- Data-mules will typically refer to Android or iOS enabled smartphones with the GAMMA application installed. They will be able to support the BLE protocol as specified in Bluetooth 4.0 onwards and have access to the Internet.

In the absence of internet connectivity, the data-mule will be able to temporarily store data until a connection has been resumed.

- A data-mule will typically have reasonably accurate location services (e.g. GPS), as well as network synced time.
- The remote server(s) will be able to handle simultaneous connections with multiple data-mules. The server will be able to dynamically scale depending on demand.

2.3 Analytics

The GAMMA platform provides analytics on the specific data that is accumulated on the cloud which are handled in a back-end server. The analytics conducted will be application-specific and can range from sole use-cases to system wide analytics containing a multitude of devices. The individual end-nodes will also be able to do limited analytics locally. This is mostly limited to data averaging and critical event reporting, to not overwhelm the network with traffic that contains little value. The information generated from the back-end analytics will be made easily available online through a web-portal or through the GAMMA phone application.

2.4 Cyber Security

To ensure asset protection and data privacy, cyber security was considered from the inception. For the scope of this platform, the attack surface is limited to the end-node and the data-mule app. We assume that there exist two levels of attackers in this space; a weak and strong attacker (Fig. 2.3). The weaker attacker is not a registered user within the system

and will attempt to infiltrate by external measures. The stronger attacker is a registered user who is either malicious or has been compromised.

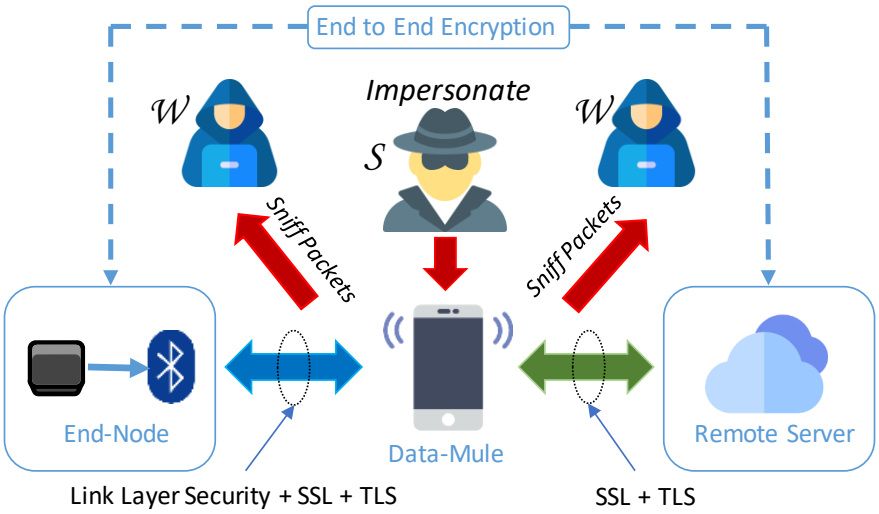

Fig. 2.3: Attacker model: weak attacker (W) can sniff packet transmissions, while strong attackers (S) can impersonate authorized users.[2]

2.4.1 Weak Attacker

The weak attacker is primarily limited to eavesdropping. This can be in the form of sniffing packets that are wirelessly transmitted, or by compromising a portion of the network that we cannot control such as Wi-Fi hotspots, routers, and networking equipment. The platform employs end-to-end encryption using AES from the end-node to the cloud. This means that at no point does the data-mule have access to unencrypted raw data and is therefore agnostic to the data that it is relaying. If these packets are intercepted, the attacker will be unable to interpret the data. This method of encryption is not enough, as there is still useful information that can be interpreted in the packet meta data: message length,

[2] Diagram content is credited to Qinchen Gu, PhD student at Georgia Institute of Technology and member of GAMMA development team.

timing, and frequency. Therefore, the system also utilizes SSL/TLS (Secure Socket Layer / Transport Layer Security) between the data-mule and the remote server.

2.4.2 Strong Attacker

The strong attacker intends to personate or infiltrate the system directly as a user. In terms of the ability to eavesdrop on the data being transmitted, the strong attacker is no different than the weak attacker since the data-mule application does not have access to unencrypted data. To prevent local data manipulation, a key-hashed message authentication code (HMAC) has been implemented on top of AES. If any data is altered the hashing function will not work, and the data will be discarded at the server end. To prevent a data destruction attack, the end-nodes will store all local data until confirmation has been received from the remote server that the data has been successfully uploaded to the cloud. Since the system is inherently delay tolerant, there is no expected latency between transmission of the data and confirmation from the server. Duplicate transmissions will therefore be made to multiple data-mules until success. By having redundant transfers, the likelihood of circumventing a malicious or compromised user is increased.

2.5 Dedicated Network Fallback

While there are multiple benefits to a DTN based communication system, it is not without drawbacks. There is no guarantee how long the duration between successful transmissions will be. The data received can also be partial or out of order, again needing an indeterminate amount of time to address missing data.

For use-cases where there were previously no sensors, limited or partial data might still be more desirable than no data at all. For applications that require more dependable means of communication, a dedicated fallback network can be employed such as a GSM or LTE radio. Rather than use this full-time, requiring a larger energy budget or costly data transfers, this communication could be set to only activate on demand or as the result of a countdown timer.

The inverse is also possible. The DTN could be used as a fallback in cases where the battery is running low and must employ more stringent power consumption. The DTN could also be utilized if cellular communication goes down or is unreliable. Regardless of the application, having multiple communication pathways opens flexibility and reliability that was previously non-existent.

CHAPTER 3

SMART UTILITY METER

For testing and demonstrating the platform, a smart utility meter was designed with GAMMA embedded in the heart of the device. This chapter details the utility of such a device in developing markets, the value gained with GAMMA, how it was implemented, and potential applications.

3.1 Background and Motivation

Adoption of smart meters in developed countries has led to greater visibility of the grid edge. In areas like Europe, deployment of smart meters is approaching 80% of the market share [16]. China is projected to hit 377 million units by 2020, and India 130 million by 2021 [17]. While these are impressive numbers in terms of magnitude, in market injection they are lagging well behind developed countries. The largest factor gating deployment is cost. The capital expenditure including equipment, maintenance, and operational costs for deployment of AMI infrastructure in India is $120 per unit [18].

Equipment installed by AMI has provided many benefits to utilities. Data gathered from end-devices can provide useful information for cloud-based analytics [19]. From these capabilities, issues such as topology estimation [20], and detection of ground fault locations [21] can be addressed faster and more efficiently than before. Further, AMI devices provide a direct benefit to utility companies by mitigating and correcting power factor and quality issues [22]. Despite these benefits presented by AMI, utilities are still faced with several challenges [23]. Hardware and labor costs remain high, and when

installed in low population areas, present comparatively little added value. Recurring costs associated with cellular modems can also hinder ROI.

The motivation behind the development of the GAMMA enabled smart meter was to provide utilities in developing countries with a means of deploying smart grid technology rapidly, easily, and at low cost. Current technologies in this sector are not suitably priced for the target demographic. Emerging markets need cost effective controllable devices which can be used to build the grid from the bottom up. A device platform capable of providing cloud-based analytics, localized and remote controllability, low communications cost, and power quality compensations could have a significant impact in developing markets.

3.2 Architecture Overview

This section describes the development and capabilities of the smart meter which is the fundamental end-device for the distribution automation platform.

The smart meter (Fig. 3.1) sits between a low voltage single-phase AC source and the desired load to be metered. For emerging markets, the maximum load considered was 10A and was sized to support 240Vac. The system is powered directly from the line through a capacitive power supply. This is used to generate a DC voltage to power the digital and analog circuitry for the meter. Voltage and current measurements are conducted by an analog front end (AFE) from Analog Devices (ADE7953). The data is then processed and managed by a Bluetooth enabled MCU from Texas Instruments (CC2640). This data is used in tandem with commands from the cloud to operate the VAR compensator, and relays.

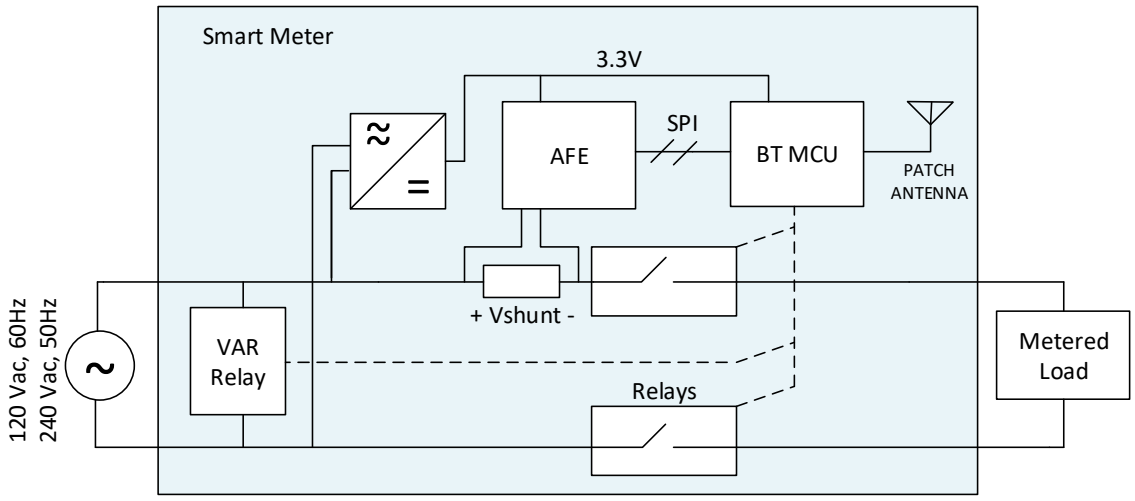

Fig. 3.1: Block Diagram for GAMMA Smart Meter

The MCU is equipped with an Inverted-F Antenna (IFA) built into the PCB. By incorporating the antenna into the PCB, expensive connector and rubber-duck antennas can be omitted. The MCU will periodically advertise its MAC address and upon successful and authorized connection, will exchange data with the cloud via the mule application. (RF performance and design will be covered in greater detail in the next chapter).

3.2.1 Measurements

Since the expected amperage is relatively low, a high-precision low resistance shunt-resistor in the main current path is used in lieu of a current transformer to drive cost down. The voltage drop across this resistor is used to measure total load current. Since the voltage present at this resistor is significantly high compared to the neutral connection, the DC voltage rail is referenced to the AC line rather than neutral. This presents a small voltage drop from either end of the shunt resistor to the analog ground. The AFE also monitors the input voltage at the AC neutral line by stepping down the voltage via a

resistive network. Both the voltage and current inputs are interfaced with a sigma-delta analog digital converter (Σ-Δ ADC).

The voltage and current measurements are used to generate interrupt signals such as reverse power flow detection, as well as voltage and current zero crossings. The data collected by the AFE is sent to the MCU via a Serial Peripheral Interface bus (SPI). There the MCU can process the data further into rolling averages, power and energy consumption, event detection, manage account balances and operate the relays.

Active power *P* for a high power-factor load is calculated by:

$$P = \frac{1}{nT}\int_0^{nT} \sqrt{2}V_{RMS}\sin(\omega t)\cdot\sqrt{2}V_{RMS}\sin(\omega t)\cdot dt \tag{1}$$

$$P = \frac{1}{nT}\int_0^{nT} V_{RMS}\cdot I_{RMS}\cdot(1-\cos(2\omega t))\cdot dt \tag{2}$$

where, ***n*** is the number of cycles monitored, and ***T*** is the period of an individual cycle in milliseconds. If ***n*** is an integer (2) simplifies to:

$$P = I_{RMS}\cdot V_{RMS} \tag{3}$$

The root means square of the voltage and current waveforms can be written in the form of a sum of discrete data samples:

$$V_{RMS} = \sqrt{\frac{1}{N}\sum_{n=1}^{N} {V_n}^2} \tag{4}$$

$$I_{RMS} = \sqrt{\frac{1}{N}\sum_{n=1}^{N} {I_n}^2} \tag{5}$$

where V_n and I_n are individual samples, and N is the total number of samples in a measurement window. For lagging or leading loads, there exists a phase angle φ between the voltage and current periods. This can be used to define the power factor $\cos(\varphi)$. Equation (3) can therefore be rewritten as:

$$P = I_{RMS} \cdot V_{RMS} \cdot \cos(\varphi) \tag{6}$$

Once power has been calculated at a given sample period M, it can be summed to generate energy consumption E:

$$E = \sum_{k=1}^{\infty} P_k \cdot M \tag{7}$$

where P_k is an individual power calculation average over the given period M. For this application the averaging period M was set to be 4.83µs or four samples. Total energy consumed is used to calculate current account balances which are stored locally and can be relayed to the network.

3.2.2 Localized Automation

Power Factor Correction: The device has an x-capacitor at the grid input which can be brought in and out via a relay. This gives the smart meter the capability of providing 100VARs of support if the power factor or voltage quality passes a set threshold. The set-point for this threshold can be remotely updated via the cloud, and thus can be implemented in system wide volt/VAR optimization (VVO) and can provide dynamic control.

Smart Turn-Off: Account information, such as billing, is stored locally on the device's flash memory and can be synced with the cloud. The device can locally calculate energy

consumption and subtract that from a running balance. Users can be alerted about low balances. If the remaining amount runs out, the device can issue a disconnect-of-service via the two relays at the load-side. The relays are equipped with RC snubbing discharge paths to ensure safe disconnect (Fig. 3.2). Once the account balance has been refreshed via the cloud, the relays are reconnected, and service can continue.

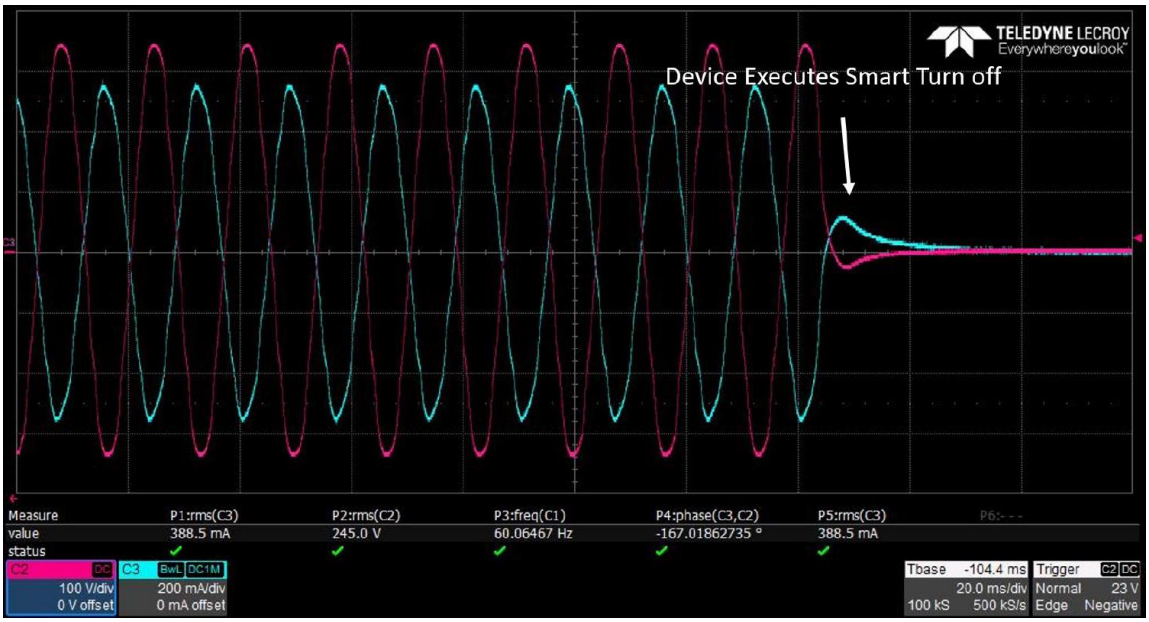

Fig. 3.2: Current (cyan) and voltage (magenta) waveforms for a capacitive load during remote shutdown. The RC snubber provides a safe transition to a null state.

Smart Breaker Action: Similarly, the device can also set thresholds for both voltage and current. Since the end-node is continuously monitoring these values, the device can safely disconnect before damage occurs (Fig. 3.3). Like with power factor correction, this threshold can be set via the cloud or in certain applications by the user to limit energy consumption or for protection.

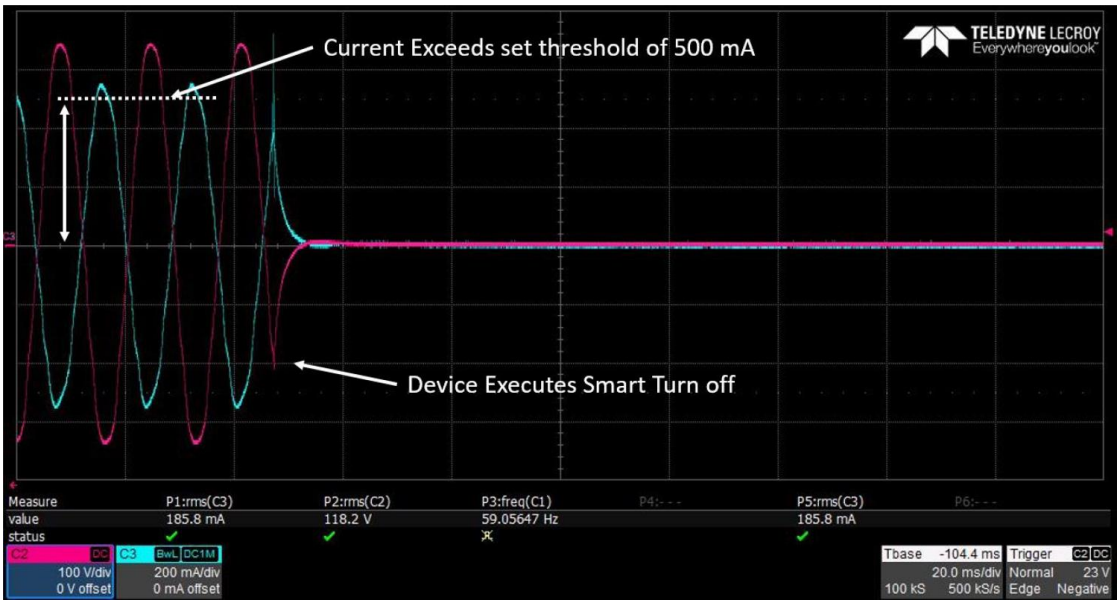

Fig. 3.3: Once a current threshold has been exceeded, the device can disconnect the load from the grid.

Theft Protection: The smart meter senses whether there is voltage present at the output to the load. If the relays have been set to disconnect from the load, yet a voltage remains at the output the device knows that it has been bypassed. Since both relays are normally open, electrical failures will most likely result in an open circuit rather than a short. This is used only to sense whether a voltage is present and is not used for measurements or metering. As a result, the input voltage signal can have a very low sampling rate and does not need extra calculation past a Boolean result.

The cloud can also remotely monitor equipment theft. The device's physical location is stored on the cloud during set-up via the data-mule's GPS coordinates. If a mule connects to the device in sufficiently different location, the cloud will be able to detect that it has changed locations.

3.3 Hardware Prototype

The schematic capture and layout for the board were designed in Eagle CAD. The final product was fabricated on a six-layer PCB, with a form factor of 12 x 12.5 cm (Fig. 3.4). The board contains several flat packages, fine-pitched pads, and small passive components. As a result, these were built and assembled by a board-house. Since the AFE is extremely sensitive to noise and relays and digital systems are inherently noisy, great care was taken in the PCB design to ensure good signal and power integrity.

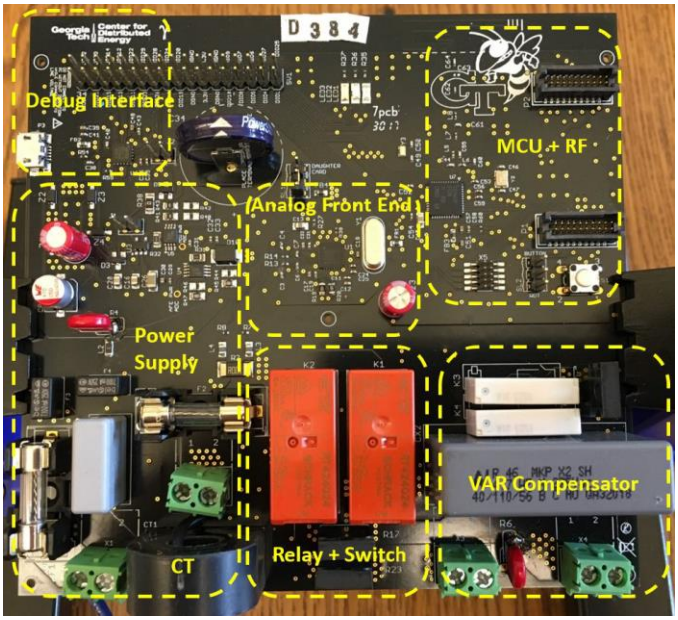

Fig. 3.4: GAMMA Smart Meter hardware with system blocks highlighted

3.3.1 Mixed Signal Grounding

Grounding schemes are undoubtedly one the most difficult and often overlooked aspect to PCB design. It is also one of the most common and pervasive sources of signal integrity issues and design failures. Unlike schematic design, where conceptual symbols are neatly laid out and fundamental problems can be readily caught in a design review;

layout requires an intimate knowledge of the system, and where currents and voltages are expected to propagate. These intricate flows often cover several overlapping layers and can be difficult to visualize how they fit together and interact with near-by circuits. It is a complex problem and can drastically change with no discernable impact on the visualization of the schematic. The problems that arise are dependent on unique physical geometries of the layout and thus don't neatly follow conventional typologies. Quality grounding and power connections can and must drive the entire layout philosophy of the design.

The disconnect between schematic and layout is further intensified by the homogenous treatment of supply and grounding connections by the schematic representation. What we call ground or V_{DD} only truly exist at one specified location. These are ultimately ideal reference points, but these points conceptually start to change once they become planes or traces on the PCB. Two separate circuits might be said to be in parallel and share the same supply nodes but will have different measurements in the lab.

Every plane will inherently cause parasitic attributes that will impact voltages and currents along the line. The ground plane is especially bad as it serves as the return path for all currents within a subsystem regardless of which supply they generated from. The type and typology of the parasitic components is directly impacted by the geometric layout. Take an example of a simple system comprised of a single DC voltage supply, a digital and an analog circuit that are tied in parallel to a common ground. The layout engineer in this case chose to position the analog system close to the voltage source, and the digital system further along the board.

The ground connections on the analog circuit are not at system ground but rather a voltage node that we will call analog-ground (AGND). Likewise, the digital ground connection is at a different node that we will call digital-ground (DGND). The voltages at these nodes are dependent on the transient currents that occupy them (Fig. 3.5).

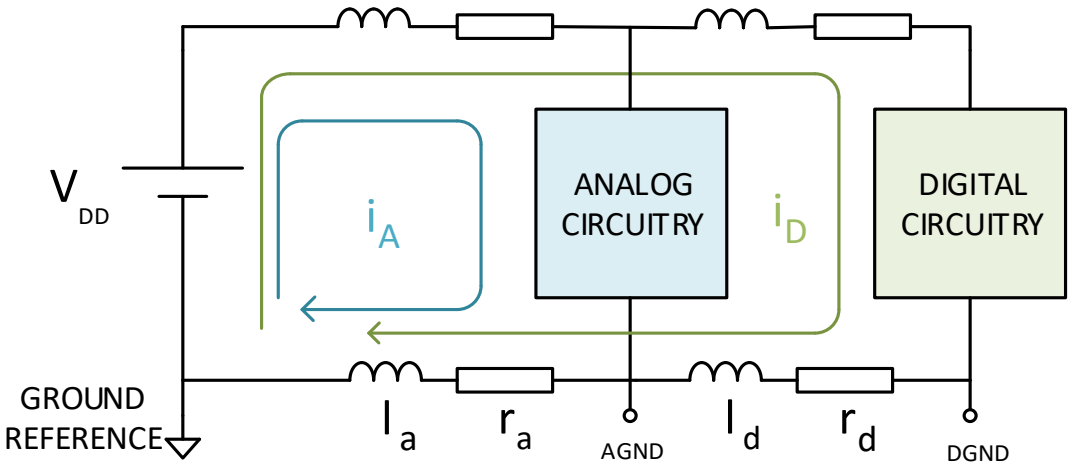

Fig. 3.5: Mutual return planes can cause offsets between analog and digital grounds relative to the system ground reference.

The node voltages can be written as:

$$V_{AGND} = r_a \cdot (i_A + i_D) + l_a \left(\frac{di_A}{dt} + \frac{di_D}{dt}\right) \tag{8}$$

$$V_{DGND} = r_a \cdot (i_A + i_D) + l_a \left(\frac{di_A}{dt} + \frac{di_D}{dt}\right) + r_d \cdot i_d + l_d \frac{di_D}{dt} \tag{9}$$

where $\boldsymbol{r_a}$ and $\boldsymbol{r_d}$ are the parasitic resistances due to ohmic losses, $\boldsymbol{l_a}$ and $\boldsymbol{l_d}$ are parasitic inductances created by current loops, and $\boldsymbol{i_A}$ and $\boldsymbol{i_D}$ are the currents present in the analog and digital circuits.

Even though this is a simple system with only two currents and a shared return plane, the impact on the relative ground can get complicated fast. This is further agitated

by the addition of a several currents and more complicated parasitic typologies caused by the layout. The impacts on the voltage supply pins can be calculated by a similar process.

Despite being placed close to the supply source, the analog ground is still impacted by the currents flowing through the digital circuitry. The digital ground contains the same problems present at the analog reference plus the addition of the digital currents running through the remaining length of the return plane.

In some designs the values of the parasitic components are relatively small, or the currents through them might also be small. In these cases, it might be okay to neglect how the layout will impact the functionality of the design. For more complicated structures, higher currents, and sensitive circuitry it is imperative that these impacts be mitigated and decoupled from one another.

One method is physically separating the return paths to force current to flow through specific portions of the board and later join the system ground at a common point (Fig. 3.6). This typology is often called a star ground and is useful as it decouples both the parasitic components, as well as the currents.

The node voltages at these references can now be defined as:

$$V_{AGND} = r_a \cdot i_A + l_a \frac{di_A}{dt} \tag{10}$$

$$V_{DGND} = r_d \cdot i_d + l_d \frac{di_D}{dt} \tag{11}$$

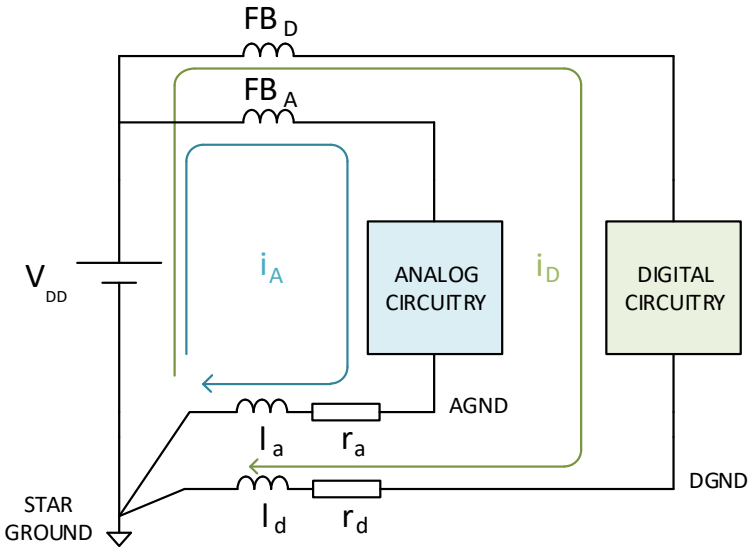

Fig. 3.6: Schematic representation of a star ground. Analog and digital return planes are separated until the star connection point.

The two reference points have now been satisfactorily decoupled from one another and can be more directly controlled. The supply voltages can also be decoupled by including a ferrite bead along the current path, or if needed, by having two separate supplies; one for the analog subsystem and one for the digital.

3.3.2 AFE Layout

The AFE on the smart meter is very sensitive to noise. The ADC pins can reject up to 25mV of common mode noise relative to analog ground. Since the AFE contains both analog and digital communications on the same die, the IC itself is a mixed signal system. To mitigate noise present at the analog ground, it is necessary to decouple the analog and digital currents within the AFE subsystem, as well as decouple the cumulative AFE currents from the entire system.

The analog return path is diverted to a dedicated return plane on an inner layer in the PCB through vias (Fig. 3.7). Since the relative analog and digital grounds are not separated by a component, they are technically the same electrical net and must be manually separated by cutouts in the return plane. The digital ground is less sensitive and occupies all remaining space through a ground pour on all layers.

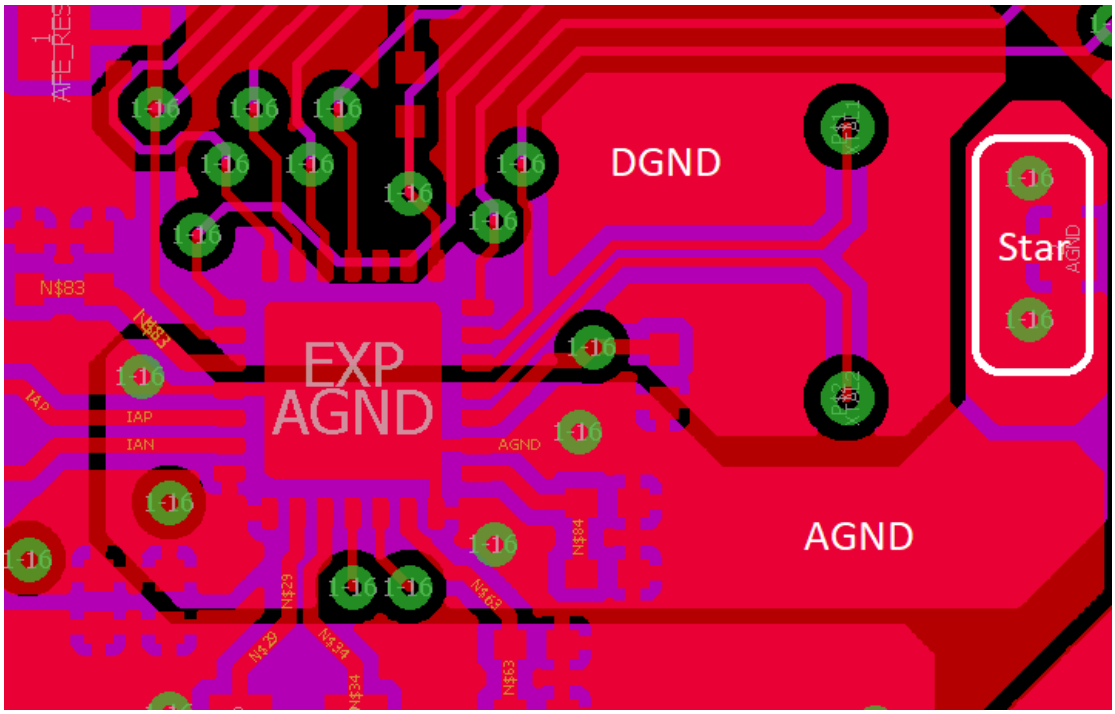

Fig. 3.7: Star ground typology for the AFE. The analog return plane is contained in an inner layer (magenta), while the digital plane occupies the remaining space.

The AFE's star ground is further separated from system ground by creating an island which connects to the system ground via a ferrite bead (Fig. 3.8). Having only one connection to ground guarantees that cross currents will not flow through the island bypassing sections of the system ground. Only currents passing through the AFE will flow through the ferrite bead.

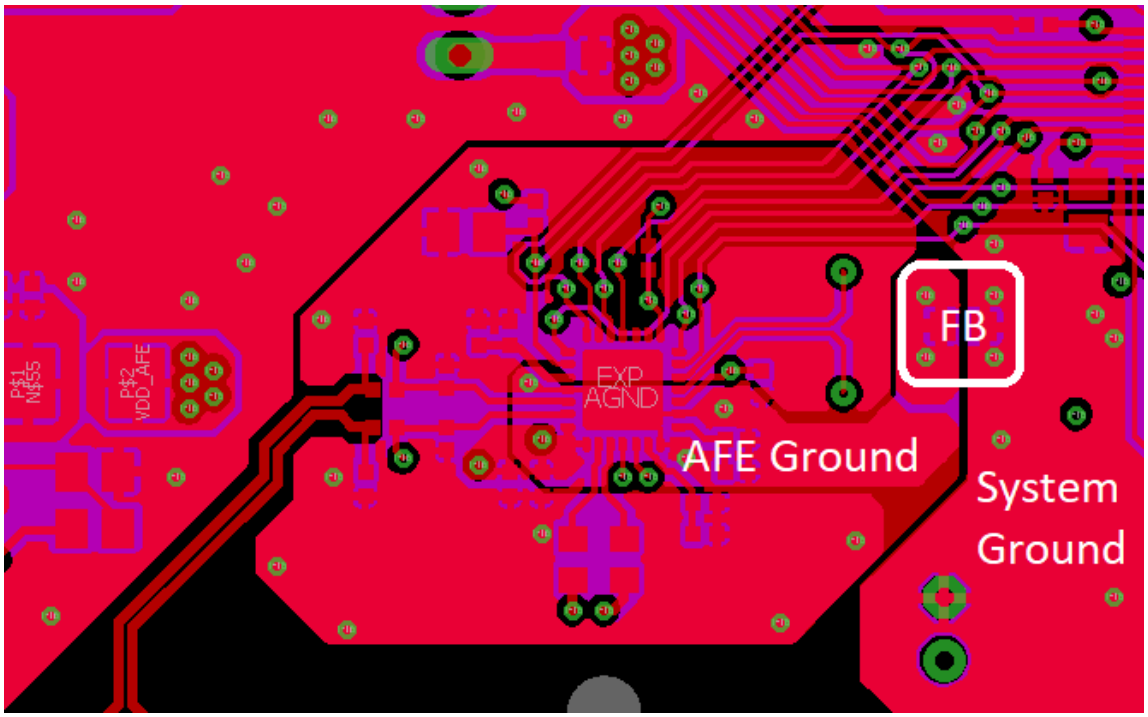

Fig. 3.8: The digital and analog grounds for the AFE are islanded by a ferrite bead.

The digital signals going to the MCU cross the moat that separates the AFE ground and the system ground. This will cause the returning current flowing through the ferrite bead to take a longer and indirect path. The elongated return path will increase the parasitic loop inductance seen by the digital ground and introduce noise to the system. This is ultimately permissible, as the digital circuitry has a much higher noise tolerance and has been at least partially decoupled from the analog system.

In lab tests the analog ground on the AFE had a common mode noise of ±8mV relative to the shunt resistor, well within the target range of ±25mV. Most of this voltage appears across the ferrite bead due to its DC resistance and is unlikely to be further improved by PCB design.

3.4 Performance

To simplify calibration, the device was initially powered by a controlled and isolated AC power supply. This provided relatively clean sinusoidal waveforms and the provided isolation made the phase and neutral interchangeable. For sensor calibrations, the smart meter was attached to a 100-watt lightbulb with a power factor near unity. By removing the phase calculations, the ADC output could be calibrated using only active power without the need to worry about power factor. Once the voltage and current measurements had been calibrated against known values, the resistive load was exchanged with a capacitive load, which was used to calibrate reactive power and phase measurements.

3.4.1 Hardware Performance

In metering applications, the sensor data is used for billing purposes and should be as accurate as possible, typically within 1%. After calibration of the ADC outputs, the smart meter was able to achieve a 0.5% accuracy for both voltage and current, with a resolution of 500mV and 17mA. Phase resolution had a little more jitter since it is dependent on two separate measurements, each with their own margins of error. Typical values were between 0.020 and 0.024 degrees. For RF, the Bluetooth range under line of sight conditions was around 95 meters. Further specifications are in Table 3.1.

Table 3.1: Energy meter specifications

Parameter	Value
Form Factor	15 cm x 15 cm x 3 cm
Input Range	120 V_{RMS} 60Hz, 240 V_{RMS} 50Hz
Input Tolerance	±20%
Voltage Resolution	500 mV
Voltage Accuracy	±0.5%
Max Supported Load	8 A_{RMS}
Current Resolution	17 mA
Current Accuracy	±0.5%
ADC Word Length	24 bits
ADC Sampling Rate	895 kHz
Bandwidth	1.23 kHz
Phase Resolution	0.02°
VAR Support	100 VAR
Bluetooth Range (LoS)	95 m

3.4.2 Platform Performance

One of the meter prototypes and a data-mule were taken to Accra, Ghana and operated for 8 hours with a 100W lightbulb. The mule app was able to communicate with the smart meter and upload its GPS location and metering data to the cloud (Fig. 3.9).

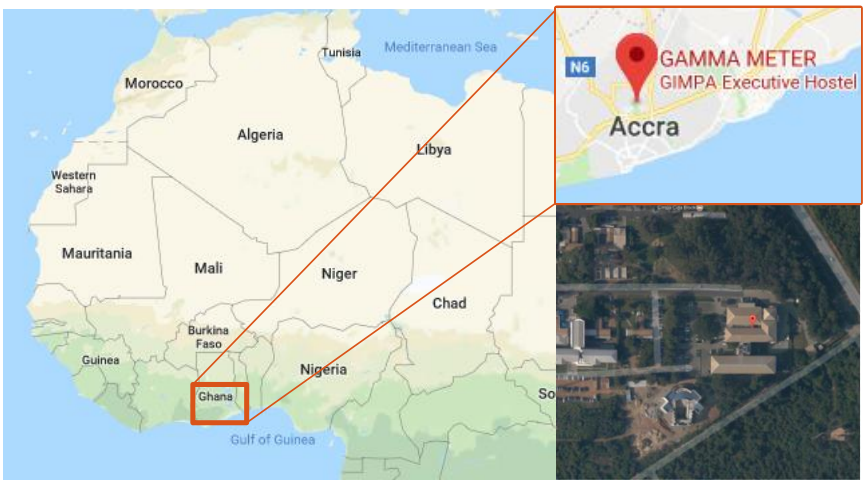

Fig. 3.9: GPS Location of device in Accra, Ghana

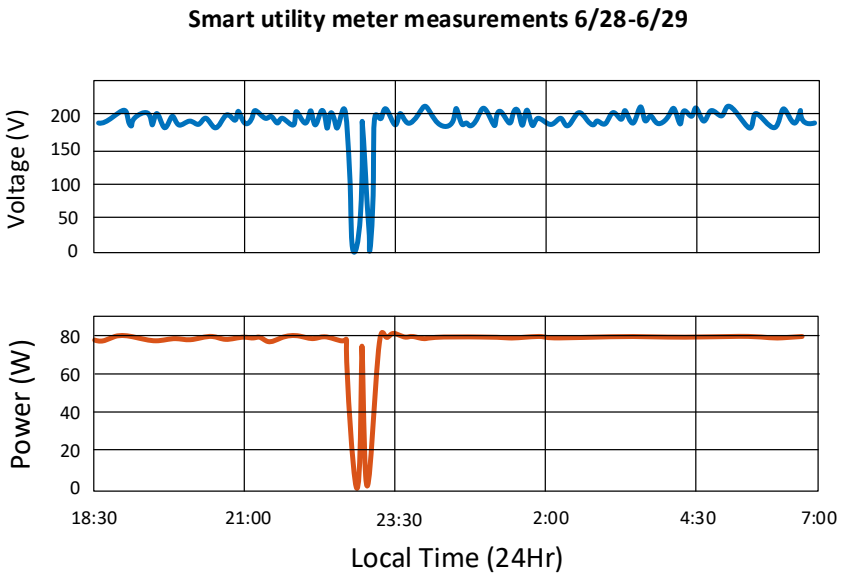

Fig. 3.10: Metering data from Accra. Two remote relay commands were sent at 23:00 and 23:15.

While communicating with the data-mule, commands to switch the power load off and back on were issued remotely in Atlanta Georgia. The commands were issued twice, once at 23:00 in Ghana, and once again fifteen minutes later (Fig. 3.10). The server received confirmation that the commands were executed, and the resulting metering data verified that the load had been toggled twice within a fifteen-minute period.

3.5 Potential Applications

As mentioned previously, the smart utility meter is much more than a node. With cloud connectivity, and on-board intelligence the end-device can operate as a utility node adding voltage support to the gird. Local memory can also be used for account billing, remote disconnect, and theft detection. These features open economic opportunities for micropayments for low income customers that would otherwise be left out due to high upfront costs.

CHAPTER 4

DESIGN REUSE AND RF OPTIMIZATION

To increase design flexibility and platform performance, the core technology of GAMMA was redesigned and placed on a small form factor daughter card. This chapter details the development of this device, RF design and performance.

4.1 The Kernel Concept

After the proof of concept for the communications system had been established by the smart utility meter, it became evident that the PCB layout for the MCU and RF front-end would be time-consuming and resource heavy to repeat for every embedded design. While there are application specific aspects for each application, the core components of the communication system remain the same across the entire platform. To expedite development, the communications portion of the design was condensed into a daughter card that will further be referred to as the Kernel.

4.2 Architecture Overview

The Kernel, as depicted in Fig. 4.1, consists of the Bluetooth MCU, necessary power management, flash memory, watchdog timer, analog amplifiers for signal conditioning, and an external power amplifier with patch antenna. By consolidating the core of the BT platform onto a daughter-card, the flexibility, price and time-to-market of new applications is dramatically improved. Rather than needing six layers or impedance control on the entire board, the more cost-heavy aspects of PCB design can be limited to a small area. With a bulk of the design constraints off-loaded onto the Kernel, new

applications need only to provide a board which offers DC power and peripherals to interface with the module. This design philosophy is similar to that of GSM modems packaged on their own PCBs with either LGA pads or castellated sockets.

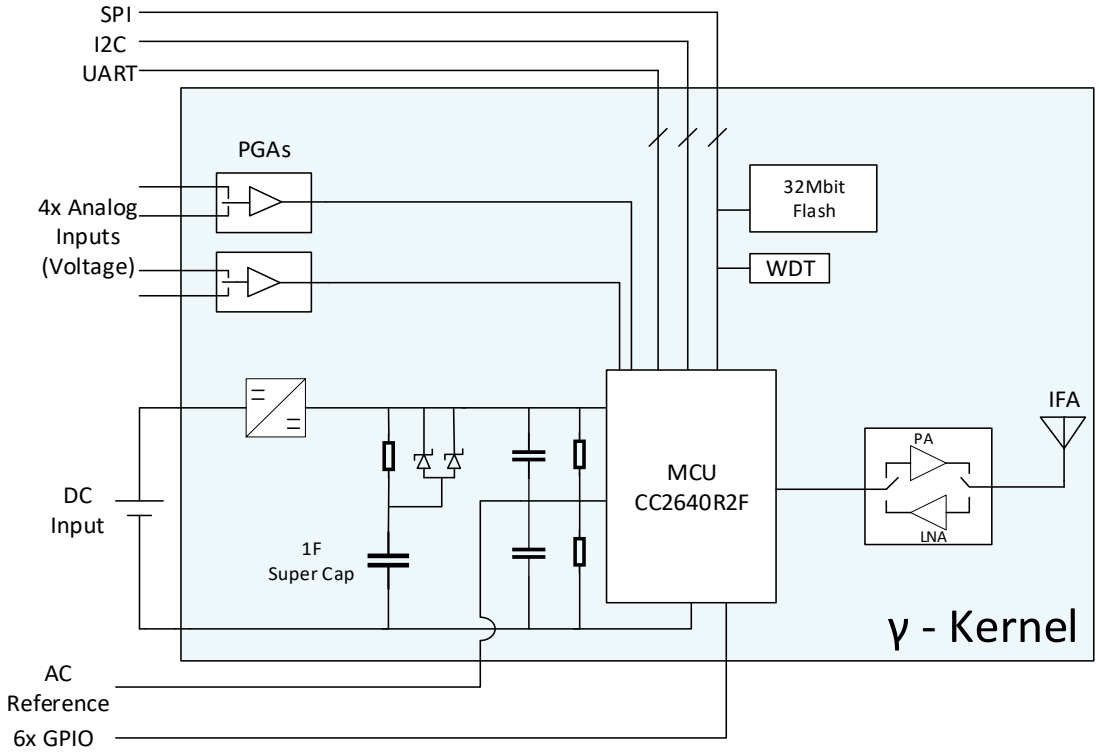

Fig. 4.1: Kernel Block Diagram

4.2.1 Outage Contingency

For several applications, it might be necessary to maintain autonomy for a short duration after a power failure. This could be useful for event reporting or dying gasp communications. Most devices in the IoT space use coin cell batteries or small rechargeable lithium-based batteries. These can provide utility under some specifications but aren't quite universal. Coin cell batteries are limited to single uses and require manual

replacement for continued use. Lithium provides extra flexibility as it can be recharged but is infamous for its limited longevity.

A compromise between these two options was sought by fitting the Kernel with a 1F super capacitor. The capacitor is not limited to a single use and can be operated for many years past a lithium battery. The main disadvantage presented by the super cap is that it will typically only provide 3-25 minutes of autonomy; depending on the power budget of the system and code. The Kernel can still be fitted with a coin-cell or lithium battery but will require external connections to the DC input to do so. Since every application will require a main application board that is tailored to each use-case, this was a fair compromise between cost and function.

The on-board power management was designed with contingency in-mind. The LDO was chosen to support a back voltage at the output. This is specifically to avoid damaging the LDO when the voltage remains up at the output, yet the input is down. In prior designs, a diode in the main current path was used to block this voltage. However, the power rail took a voltage-drop as a result, and the super-capacitor would not charge to full rail voltage. To limit the surge current from the capacitor during initial charging, a 390-ohm resistor was placed in series with the capacitor. Schottky diodes in parallel with the limiting resistor provide a low impedance current path back to the main rail. To limit the current dependent voltage-drop across the diode, two were used in parallel. The impact of the voltage across the diodes was further mitigated by adjusting the output of the LDO to 3.4V, so that rail voltage would drop to the nominal value of 3.3V during outage.

The MCU has an input range of 1.8V-4V and can continue to operate as rail voltage declines. An on-die voltage regulator provides a 1.2V reference used for ADC

measurements. The MCU can therefore monitor its own rail voltage and go into power saving modes when it detects a declining rail voltage.

4.2.2 Analog Inputs

The Kernel provides four analog voltage inputs that are multiplexed by a programmable gain amplifier (PGA). The tunable gain provides a larger voltage input range to increase design flexibility. The output of the PGAs goes to ADC capable GPIO pins on the MCU, and the inputs of the PGAs can be toggled over the SPI communication bus.

The inputs to the PGAs can be either DC or AC. In the case of an AC input, where the voltage can swing negative, an AC reference is available on the Kernel. The reference is generated by a resistor divider which provides half rail voltage to give AC signals a sufficient DC offset. Since the DC offset is present at the input of the amplifier, it will also be amplified with the AC signal. It is therefore necessary to set the gain of the amplifier to unity. As a result, AC input is limited to the RMS equivalent of half-rail voltage or $1.2V_{RMS}$. If a larger input range is required an external resistor network must be implemented to step the voltage down to 1.2 V_{RMS} or lower.

4.2.3 Digital Peripherals

The Kernel is fitted with 32Mb of external flash memory. For continuous voltage and current measurements, this is equivalent to about 6 months of local data storage. The MCU is equipped with a watch dog timer (WDT), which can provide an external reset

signal if the MCU is unresponsive. The timer for the WDT is a simple RC circuit, and can be modified as needed.

Several of the GPIO pins have been allotted for standard communication protocols; these include SPI, I2C, and UART. The I2C and UART can be repurposed as generic GPIO pins, however since the SPI lanes are used locally they must remain SPI connections. These communication pins, along with 6 GPIO pins are accessible through header pins.

4.3 RF Design

Wireless communication lies at the heart of the Kernel design and is the linchpin in the GAMMA architecture. The platform depends on the ability of the device to communicate with as many mules as possible and must maximize the range of communication within FCC regulations. As stated in the previous section on the smart utility meter, we were able to achieve 95 meters of operable range with the MCU and patch antenna. While this is incredible for consumer-end applications, it severely limits the region of communication of the GAMMA device.

For the Kernel, an external power amplifier (PA) and low noise amplifier (LNA) were positioned between the MCU and the antenna to maximize output power and receiver sensitivity. The PA increases the MCU output from +5 dBm to +21 dBm, and LNA improves the receiver sensitivity from -97dBm to -100 dBm. This dramatically improves the uplink budget, with modest improvements to the downlink budget.

4.3.1 Impedance Control

Every trace on PCB presents a characteristic impedance that is the direct result of transmission line parasitics. These can be modeled as an RLC circuit which represents an elemental length of a transmission line (Fig. 4.2). The characteristic impedance of the transmission line is the ratio of the instantaneous voltage and current of a single wave in the absence of reflections. Alternatively, it is the effective input impedance of the transmission line when its length is infinite. If a finite length of transmission line is terminated in a load having the same impedance of the characteristic impedance, the wave will behave as if the line is infinite and will not reflect.

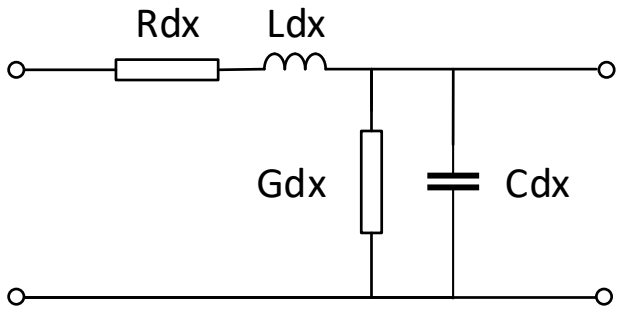

Fig. 4.2: Equivalent circuit of an elemental length of a transmission line.

The value of the characteristic impedance can be calculated using the telegraphers equation:

$$Z_0 = \frac{V(x)}{I(x)} = \sqrt{\frac{R + j\omega L}{G + j\omega C}} \tag{12}$$

where R is the resistance per unit length, $\boldsymbol{L}$ is the inductance per unit length, $\boldsymbol{G}$ is the dielectric conductance per unit length, $\boldsymbol{C}$ is the capacitance per unit length, and $\boldsymbol{\omega}$ is the angular frequency of the wave. For systems with low line resistance, and no dielectric loss,

R and ***G*** will be very small compared to ***L*** and ***C***. This will simplify the characteristic impedance to:

$$Z_0|_{R\to 0,G\to 0} = \sqrt{\frac{L}{C}} \tag{13}$$

The characteristic impedance can now be treated as frequency independent, which is desirable for mixed or variable frequency signals.

While the characteristic impedance might be stable over a wide range of frequencies, this does not mean that the impacts of the impedance are the same across the frequency spectrum. The transmission line is still described per unit length and is dependent on the physical length of the line relative to the wavelength of the propagating wave. Lines shorter than a quarter wavelength are considered electrically short, the impedance seen at the load dominates the circuit [24]. As the physical length of the line approaches a quarter wavelength and beyond, the line becomes electrically long, and transmission line effects must be considered.

For many frequencies in the low to mid-megahertz range, this can be 150 centimeters to nearly 75 meters. For PCB designers, this is typically not something to worry about, and thus the specific value of characteristic impedance can largely be ignored. Once signals pass into the high megahertz, and gigahertz range these resonant lengths start to become small enough that they begin to impact the system. However, this is not exclusive to high frequency systems. For power distribution where harmonics can be several hundred hertz, transmission line effects can start appearing after only a few kilometers.

Bluetooth occupies the 2.4 GHz ISM band, along with Wi-Fi, Zigbee, WirelessUSB, controls for RC vehicles, and commercial microwave ovens. A quarter wavelength at this frequency is about 3 cm and must be carefully considered while designing an RF system. The characteristic impedance of any traces carrying these frequencies must be controlled to match the impedance that is required by the driver and the load. Wireless ICs are typically designed around a specific characteristic impedance and are very sensitive to deviations from the control. Improperly matched traces can result in unwanted reflections and standing waves. This will in turn decrease power transfer to the antenna, source more current from the PA, and increase losses in the matching network. These factors will negatively impact system performance and must be mitigated through design.

4.3.2 Coplanar Waveguide with Ground

The PCB trace leading to the antenna is routed over a solid ground plane separated by a dielectric pre-preg. The trace is also surrounded by a solid ground layer on both sides separated by a gap. This configuration is referred to as a coplanar waveguide. The cross section of the waveguide can be seen in Fig. 4.3, where $\boldsymbol{h}$ is the height of the dielectric layer, $\boldsymbol{a}$ is the trace width, and $\boldsymbol{b}$ is the total distance between both gaps. For all cases considered, the dielectric constant $\boldsymbol{\varepsilon_r}$ will be 4.2.

The characteristic impedance of waveguide [25] can be calculated by:

$$Z_0 = \frac{60\pi}{\sqrt{\varepsilon_{eff}}\left(\frac{K(k)}{K(k')} + \frac{K(k_1)}{K(k_1{}')}\right)} \tag{14}$$

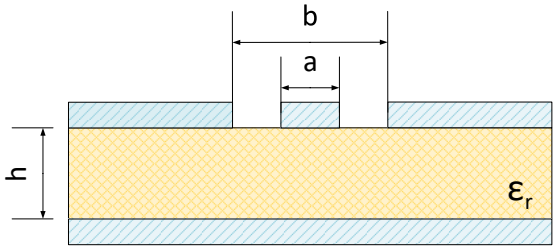

Fig. 4.3: Cross section of a coplanar waveguide

Where the values of k, k', k_1, and k_1' are defined as:

$$k = \frac{a}{b} \tag{15}$$

$$k_1 = \frac{\tanh\left(\frac{\pi a}{4h}\right)}{\tanh\left(\frac{\pi b}{4h}\right)} \tag{16}$$

$$k' = \sqrt{1 - k^2} \tag{17}$$

$$k_1' = \sqrt{1 - k_1^{\,2}} \tag{18}$$

These can then be used to calculate the effective dielectric constant:

$$\varepsilon_{eff} = \frac{1 + \varepsilon_r \frac{K(k')}{K(k)} \frac{K(k_1)}{K(k_1')}}{1 + \frac{K(k')}{K(k)} \frac{K(k_1)}{K(k_1')}} \tag{19}$$

where the function $K(x)$ is an elliptical integral of the first kind:

$$K(x) = F\left(\frac{\pi}{2} \middle| x\right) = \int_0^{\pi/2} \frac{1}{\sqrt{1 - x \sin^2 \vartheta}} d\vartheta \tag{20}$$

Due to multiple variations of the letter ‘k’ and pervasive use of the elliptical integral, it is strongly advised to not try this by hand. The MATLAB function ***ellipke(x)*** can be used without needing to compute the integral directly [26].

With a defined target impedance and dielectric constant, there are still three variables that are left to the discretion of the designer. Theoretically, there are an infinite number of configurations of height, trace width, and gap width which will match the target impedance. However, due to manufacturing constraints and tolerances, some configurations are better suited for design stability, flexibility, and efficiency.

4.3.3 Manufacturing Limitations

Fabrication techniques, and capabilities differ from company to company. It is therefore beneficial to know which structures and tolerances the board-house can provide prior to starting a design. Many PCB manufacturers will offer impedance control to help tune a specific trace to a desired impedance, however these will only be fine adjustments on the specifications provided in the stencil file of the PCB. They will typically not offer design suggestions or optimization.

Generally, board-houses will have a default stack-up configuration that is used unless the client inquires further [27]. Even then only a few options may be available without requiring a custom layer configuration, which can be expensive. The manufacturer for this board-spin had four available stack-ups to choose from (Table 4.1).

All layer configurations add to a final finished thickness of 1.6mm. This however is only the sum of the individual layers prior to the lamination process. Once the layers of copper, pre-preg, and solid core are pressed together, the thickness of the board will decrease by around 10%. (The final lamination thickness is different for every manufacture but is usually available upon inquiry.)

Table 4.1: Available PCB stack-ups

	Thickness (µm)			
	Stack-up			
Layer	1	2	3	4
Copper – L1	35.5	35.5	35.5	35.5
2116 – Pre-preg	150	175	190	232
Copper – L2	35.5	35.5	35.5	35.5
FR4 – Core	332	332	332	332
Copper – L3	35.5	35.5	35.5	35.5
2116 – Pre preg	396	346	316	232
Copper – L4	35.5	35.5	35.5	35.5
FR4 – Core	332	332	332	332
Copper – L5	35.5	35.5	35.5	35.5
2116 – Pre-preg	150	175	190	232
Copper – L6	35.5	35.5	35.5	35.5

The final board thickness is not enough information, as each layer will compress differently. A cross section of the final thickness should be used for measurements and calculations. For this case, the final pre-preg thickness was 2% smaller. Once the final thickness has been calculated, the tolerance of the initial height must be considered. This is typically ±10% in accordance with IPC-6012 standard [28].

Trace and gap widths depend on minimum feature sizes, deposition resolutions, and clearance requirements. The minimum line width and spacing were both 3 mils, or 72µm with a resolution of 50 µm and a tolerance of ±25µm [29]. Using the available dielectric thicknesses, trace resolutions, and tolerances a parametric sweep of the controlled impedance can be used to get an idea of the sensitivity of certain configurations.

A parametric sweep was conducted for a fixed trace width of 300µm and the four heights available (Fig. 4.4); the total gap width, ***b***, was treated as a slack variable.

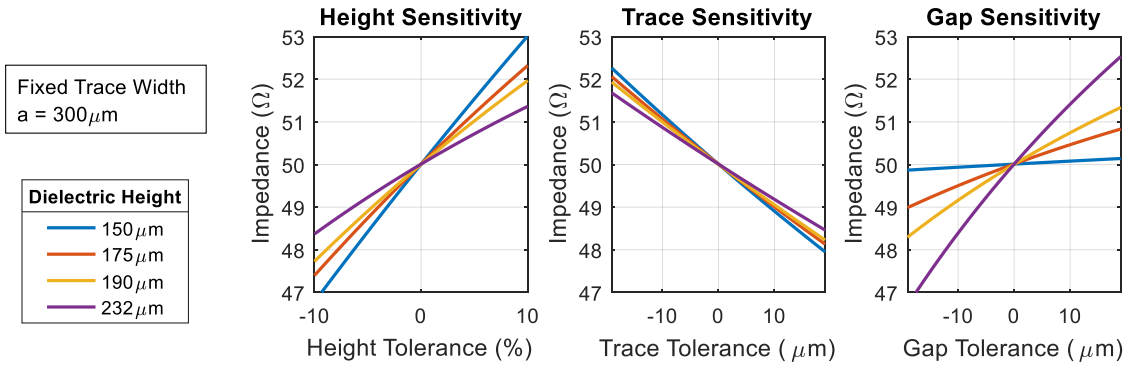

Fig. 4.4: Impact of parameter tolerances on impedance for a given trace width

Some immediate relationships begin to emerge once plotted. Trace width sensitivity remains relatively constant regardless of configuration. However, there is a clear inverse relationship between height and gap sensitivity. While a height of 150µm is almost uniformly 50 ohms across various gap lengths, it is the most sensitive to variations in height. Likewise, a height of 232µm was less sensitive to height fluctuations but was the most sensitive to gap width.

Running the same analysis but fixing the dielectric height yields comparable results (Fig. 4.5). Trace sensitivity is uniform across multiple widths, and there exists an inverse relationship between height and gap sensitivities.

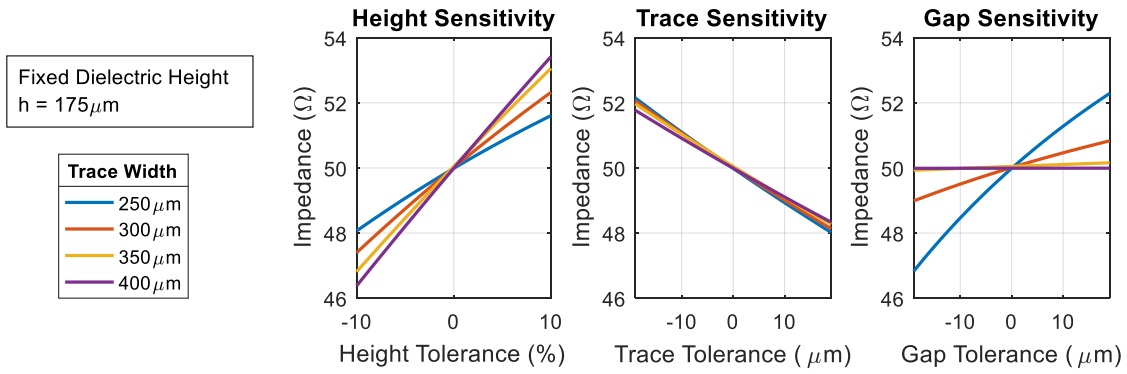

Fig. 4.5: Impact of parameter tolerances on impedance for a given dielectric height

The extremities of gap width and dielectric height exhibit both the best and worst-case sensitivities; this suggests that the values near the middle of these ranges should provide the best all-around sensitivity. This is difficult to prove with a parametric sweep where only one variable is considered at a time and requires looking at a distribution of likely outcomes based on all parameters.

4.3.4 Probabilistic Analysis

To account for manufacturing tolerances, two random variables were introduced to the impedance calculations. These are to account for the tolerances of the lamination process, $\mathcal{L}$, and the resolution of the metal plating $\mathcal{R}$.

Lamination: the pre-lamination thickness of the dielectric is guaranteed within 10% of the requested height. We can define this uncertainty as a normally random variable $\mathcal{L}$, with a mean of 1, and a variance of 0.05*:*

$$\mathcal{L} \sim \mathcal{N}(1, .05) \tag{21}$$

$\mathcal{L}$ will be normally distributed around 1 and have an effective range of 0.9-1.1. This can now be used as a scalar for the expected height:

$$\tilde{h} = h \cdot \mathcal{L} \tag{22}$$

Trace and Gap Resolution: The resolution error is given as ± 50% of the resolution width r_{min}. We can define this uncertainty as the random variable $\mathcal{R}$, with a mean of 0, and a variance of 0.25:

$$\mathcal{R} \sim \mathcal{N}(0, .25) \tag{23}$$

Unlike the lamination error, which is a scalar of the initial variable, the resolution error is the same for every instance and will be summed with the initial value. The trace-width ***a*** can now be redefined as:

$$\tilde{a} = a + \mathcal{R}_1 \cdot r_{min} \tag{24}$$

To account for the total gap distance ***b***, we must first design the gap width ***w*** to be the distance between the trace and the ground plane (Fig. 4.6).

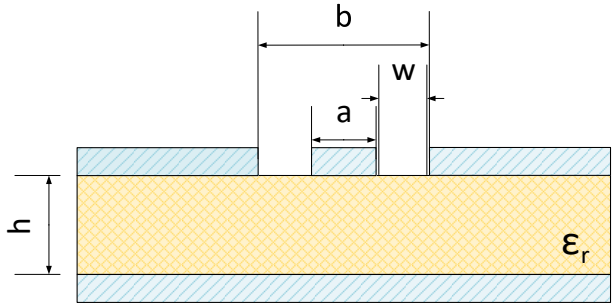

Fig. 4.6: Cross section of coplanar waveguide with added gap width "w."

We can now rewrite ***b*** in terms of ***a*** and ***w***:

$$b = a + 2 \cdot w \tag{25}$$

Accounting for resolution error and the result from (24), (25) becomes:

$$\tilde{b} = (a + \mathcal{R}_1 \cdot r_{min}) + 2 \cdot (w + \mathcal{R}_2 \cdot r_{min}) \tag{26}$$

$$\tilde{b} = \tilde{a} + 2 \cdot (w + \mathcal{R}_2 \cdot r_{min}) \tag{27}$$

The random variables $\boldsymbol{\mathcal{R}_1}$ and $\boldsymbol{\mathcal{R}_2}$ will have the same distribution, however they will be randomized independently of one another.

Simulation: A MATLAB script was used to approximate impedance distributions for various combinations of dielectric height and trace width. The script generated three

random variables, and then used these to adjust the initial values. Nested loops conducted these calculations for four widths, and four thicknesses. With three random variables, there are a vast number of possible outcomes. A sample size of two million iterations was required to get the distribution curve to converge. Once the impedance was calculated, this value was used to evaluate the transmission coefficient $\boldsymbol{\tau}$:

$$\tau = 1 - \frac{Z_L - Z_0}{Z_L + Z_0} \tag{28}$$

$$\tau = 1 - \frac{50 - Z_0}{50 + Z_0} \tag{29}$$

The transmission coefficient is a good indicator of how well the line has been matched to the target impedance of 50 ohms. A transmission coefficient of 1 indicates a perfect match, and a coefficient of 0.90 indicates that 90% of the power was transmitted to the antenna, with 10% being reflected to the source. The results from the simulation are displayed in Fig. 4.7.

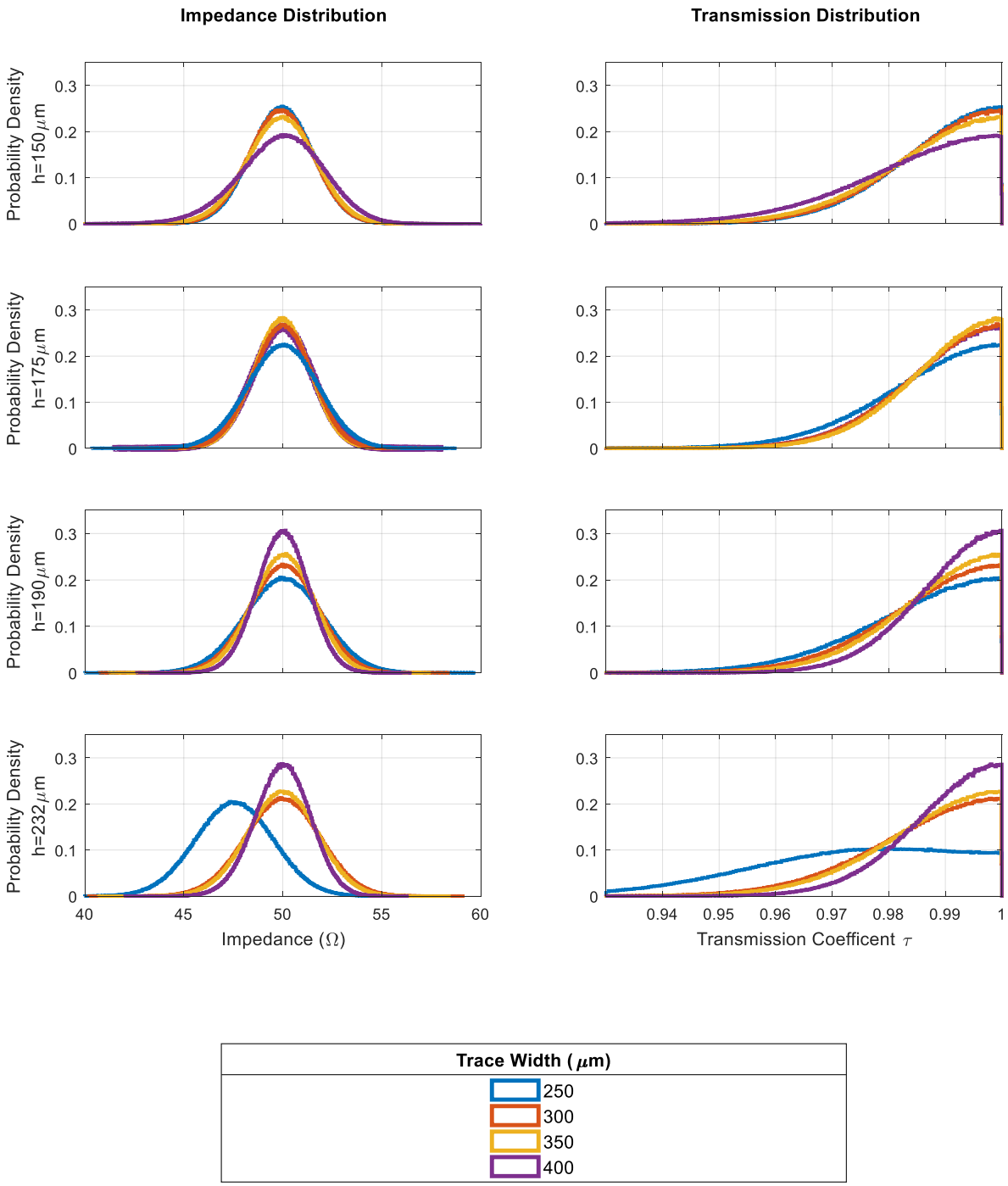

Fig. 4.7: Parametric probability distribution for impedance control

4.3.5 Choosing a Stack-up

To maximize the likelihood of a good match, the combination of dielectric height and trace width should have a high probability density at 50 ohms.

h=150µm: the smallest height has a small distribution at 50 ohms for all widths considered; around 0.18 to 0.24.

h=175µm: the intermittent height has 3 width combinations that are nearly identical peaks ranging from 0.27-0.28. The smallest width produces a lower distribution peak of 0.22.

h=190µm: a trace width of 400µm produced the most optimized combination over-all, with a peak value of 0.3. However, as trace width is reduced, the peaks begin to rapidly decline.

h=232µm: the largest height has the most diverse outcomes. There is one large peak of ~0.28 for a trace width of 400µm. However, 300 and 350µm are considerably lower at around ~0.2. Reducing the trace width further to 250µm moves the mean of the distribution to 47.5 ohms.

Even though a height of 190µm contains the optimal combination, a height of 175µm presents nearly as efficient results, but across a wider selection of widths. This configuration will grant the most design flexibility; widths can be altered between 300-400µm without needing to change the stack-up. Width flexibility is also very useful for cases where the trace width needs a transition region between the IC pad and the final desired trace width.

4.3.6 Fine-Tuning

Once the desired stack-up and trace width have been chosen, the exact parameters will be fine-tuned by the PCB manufacturer based on their capabilities. These calculations will consider the solder resist coating, weight of the copper foil, and trapezoidal shape of the trace. This is done using a calculator from polar instruments. Typically, they will fine tune the gap distance to keep the trace width close to the requested value. The final values calculated by the manufacturer are detailed in Fig. 4.8.

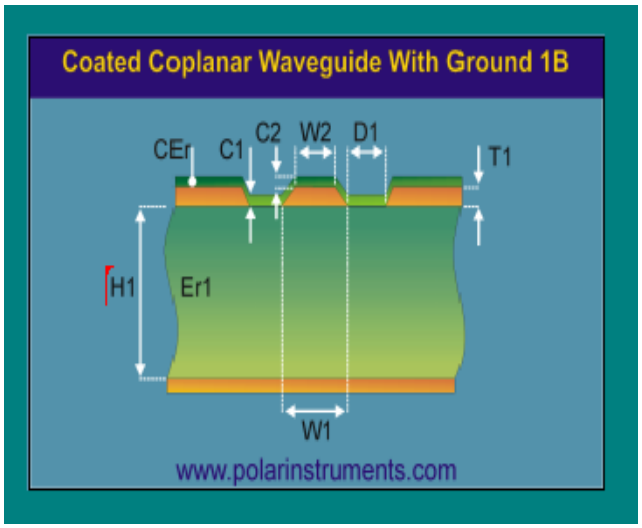

Parameter	Value
H_1	173 µm
E_{r1}	4.2
W_1	300 µm
W_2	287 µm
D_1	263 µm
T_1	42 µm
C_1	43 µm
C_2	13 µm
CE_r	3.4
Z_0	**49.61Ω**

Fig. 4.8: Impedance parameters from board-house

Using their fabrication techniques, they can configure the waveguide to have a mean of 49.61Ω. This will be close enough for practical purposes.

4.3.7 Impedance Matching Network

Once the waveguide has been calibrated to the desired characteristic impedance, it can then be used in matching the source impedance of the power amplifier, to the load impedance at the antenna (Fig. 4.9). The main goal of the impedance matching network is

to maximize power transfer to the load. This is achieved through forcing the reflection coefficient to zero at the drive frequency, filtering out unwanted harmonics and frequency components, blocking DC current, and minimizing power dissipation by utilizing passive components [30].

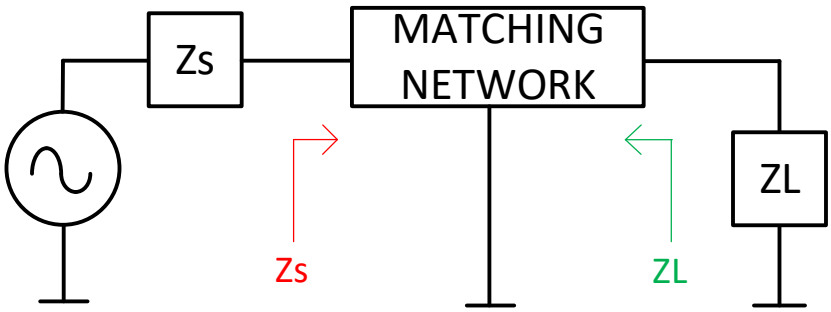

Fig. 4.9: Matching network impedances.

The load is a patch antenna designed to radiate at 2.4GHz and will have little emitted radiation for lower frequencies. However, frequencies higher than the drive frequency will have resonant paths. The filtering network will therefore be an asymmetric bandpass filter, primarily filtering frequencies above 2.4GHz.

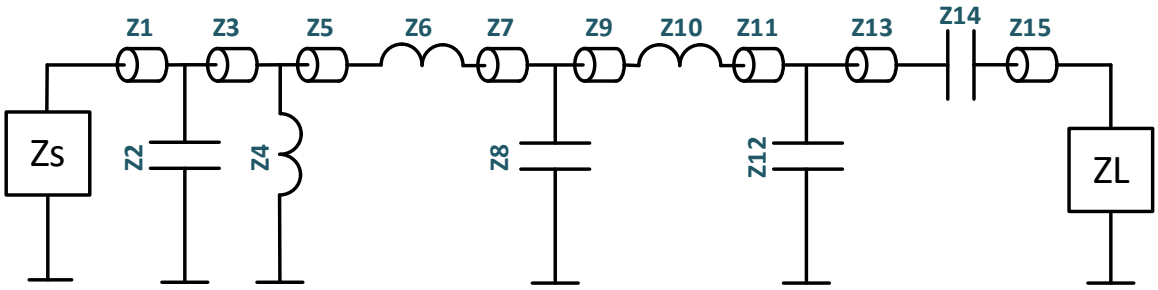

Fig. 4.10: Small signal schematic representation of impedance matching network with transmission lines.

The topology of the filtering network under small signal conditions is detailed in Fig. 4.10. The low pass portion is made up of a two-stage pi filter (***Z2***, ***Z6***, ***Z8***, ***Z10***, ***Z12***).

The last series capacitor functions as a DC current blocker before the patch antenna, and ***Z4*** provides a DC biasing point at the output of the PA.

The reactance of these components should meet 3 criteria:

1) The reactance of each component needs to be a standard value. Solving for a specific value isn't helpful if manufactures do not carry those components.
2) The chosen configuration should connect the source to the load impedance on a smith chart.
3) The specific values need to only filter unwanted frequencies, and not interfere with the desired pass band.

All three of these criteria should be met simultaneously. It is therefore suggested that both are simulated together. The most direct way is to build an initial bandpass filter and make minor adjustments using a smith chart.

The elements ***Z2***, ***Z6***, ***Z8***, ***Z10***, and ***Z12*** form the two-stage low pass filter. When added to the high pass stage, they form a bandpass filter with a lower and upper frequency cut off. Shunt capacitor values of 2-3pF are chosen for the lower frequency cut off, and 1pF are chosen for the upper cut off region. Inductor values are generally between 1 and 2 nH to help flatten the pass band. The high pass elements ***Z4*** and ***Z14*** are mostly filtering DC currents. Their values are a little more flexible but are generally higher than the other components to limit their impact on the effective impedance.

Components in these ranges were chosen to form the matching network and simulated in LTSpice. The forward voltage gain from the source to the load is displayed as a bode plot in Fig. 4.11. The bandpass filter attenuates frequencies below 300Mhz, and above 5GHz, and amplifies the frequencies in-between. The Bluetooth spectrum occupies a relatively

narrow ISM band from 2.4-4.485 GHz. The frequency response from 2.2-2.6GHz is flat, with a gain of about +5.5dB within this region. For this simulation, the antenna is treated as a purely resistive load.

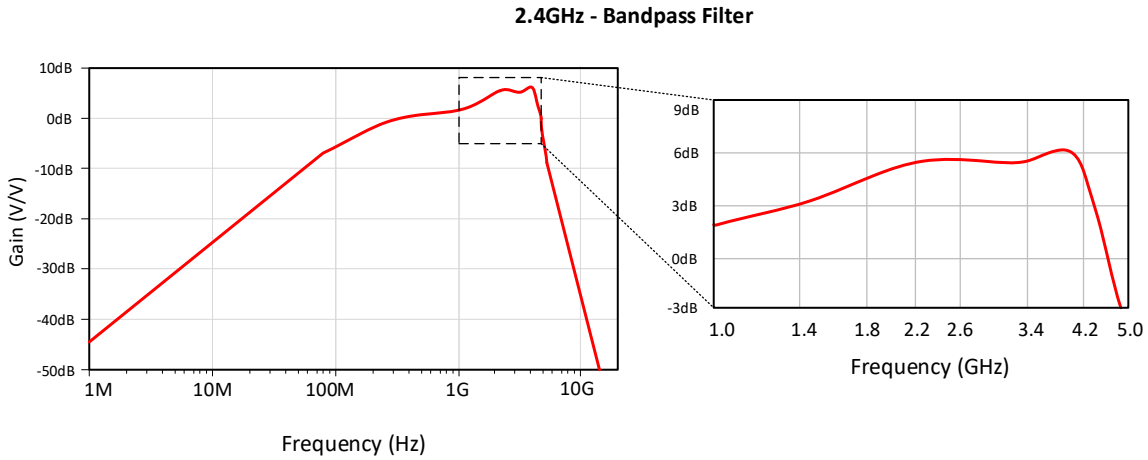

Fig. 4.11: Bode plot for the impedance matching circuit

Once a desired filter has been established, the configuration can be mapped on a smith chart to determine what adjustments need to be made. Initially, the impedance chart should only take the components into account (Fig. 4.12).

With all traces set to zero length, the final impedance is 39.5 + j17, (0.79 + j0.34 when normalized to 50). This is relatively close to the target but needs some tuning. Adding transmission lines between the components can allow the designer to shift the starting point of the curves radially around the center. By placing the components further down the transmission line, reactance can be canceled out to hit the target impedance. Fig. 4.13 shows the exact same matching configuration as before, but accounts for the spacing between components. By finely adjusting their locations on the PCB, the impedance seen at the load has been adjusted from 39.5+j17 to 50-j0.5.

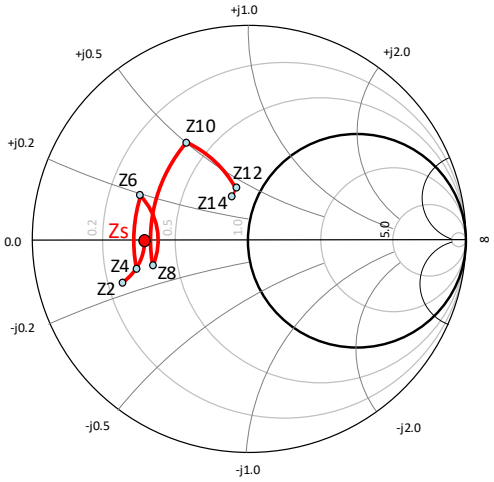

Label	Element	Value	Impedance
ZS	**Source**	**18Ω**	**0.36, j0.00**
Z2	Shunt Cap.	2.4 pF	0.25, -j0.16
Z4	Shunt Ind.	4.48 nH	0.31, -j0.12
Z6	Series Ind.	1 nH	0.31, j0.18
Z8	Shunt Cap.	2.8 pF	0.38, -j0.11
Z10	Series Ind.	2 nH	0.38, j0.49
Z12	Shunt Cap.	1 pF	0.79, j0.42
Z14	**Series Cap.**	**18.4 pF**	**0.79, j0.34**

(a) (b)

Fig. 4.12: (a) Smith chart without accounting for transmission lines, (b) table of effective impedances along the network normalized for 50Ω, and f = 2.4GHz.

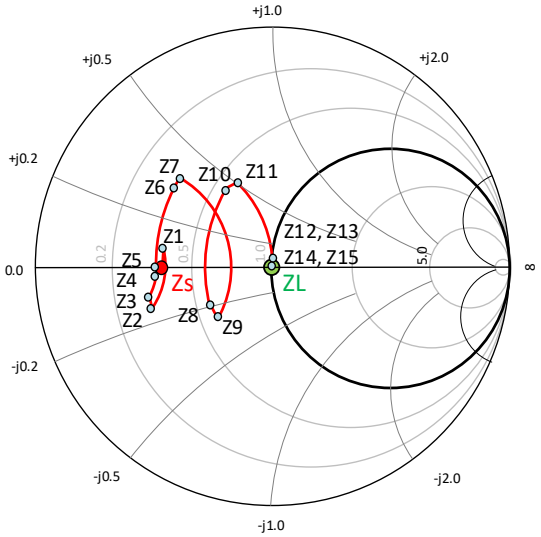

Label	Element	Value	Impedance
ZS	**Source**	**18Ω**	**0.36, j0.00**
Z1	Trans.	1.64	0.36, j0.07
Z2	Shunt	2.4 pF	0.31, -j0.15
Z3	Trans.	0.89	0.30, -j0.11
Z4	Shunt Ind.	4.48 nH	0.34, -j0.03
Z5	Trans.	0.77	0.34, j0.00
Z6	Series Ind.	1 nH	0.34, j0.31
Z7	Trans.	0.90	0.35, j0.35
Z8	Shunt	2.8 pF	0.57, -j0.28
Z9	Trans.	2.10	0.55, -j0.20
Z10	Series Ind.	2 nH	0.55, j0.41
Z11	Trans.	1.91	0.59, j0.50
Z12	Shunt	1 pF	1.00, j0.06
Z13	Trans.	0.96	1.01, j0.06
Z14	Series	18.4 pF	1.01, -j0.01
Z15	Trans.	4.19	1.00, -j0.01
ZL	**Load**	**50 Ω**	**1.00, -j0.01**

(a) (b)

Fig. 4.13: (a) smith chart matching, normalized for 50Ω, (b) table of effective impedances along the network normalized for 50Ω, and f = 2.4GHz.

Now that the characteristic impedance of the waveguide, matching network, and component placements have been finalized, scattering parameters of the network will be computed to verify that the design is operating as intended. The s-parameters of the two-port network characterize the relationship between the reflected, and incident voltage waves (Fig. 4.14).

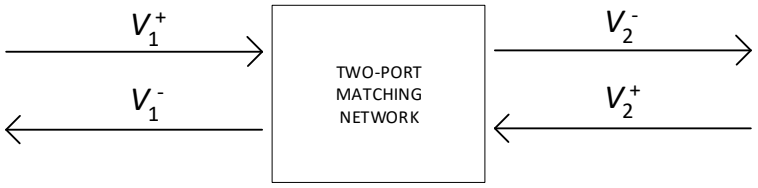

Fig. 4.14: Two port network with incident waves V1+ and V2+, and reflected waves V1- and V2-

The parameters are defined by a matrix joining the incident and reflected waves:

$$\begin{bmatrix} V_1^- \\ V_2^- \end{bmatrix} = \begin{bmatrix} S_{11} & S_{12} \\ S_{21} & S_{22} \end{bmatrix} \begin{bmatrix} V_1^+ \\ V_2^+ \end{bmatrix} \tag{30}$$

Where the s-parameters are described as:

S₁₁ **–** input port voltage reflection coefficient
S₁₂ **–** reverse voltage gain
S₂₁ **–** forward voltage gain
S₂₂ – output port voltage reflection coefficient

These can be directly plotted as functions in LTSpice, or similar circuit simulators, if the source and load are defined as ports in the netlist (Fig. 4.15).

The input port reflection coefficient ***S₁₁*** for the matching network is plotted in Fig. 4.15. The reflection coefficient has three notches where it effectively goes to zero. These occur at 2.4GHz, 4.4GHz, and 8.2Ghz. There will theoretically be very little reflection at

our desired driving frequency. The reflection coefficient is relatively higher for 2nd and 3rd harmonic rejection: 4.8GHz and 7.2GHz respectively.

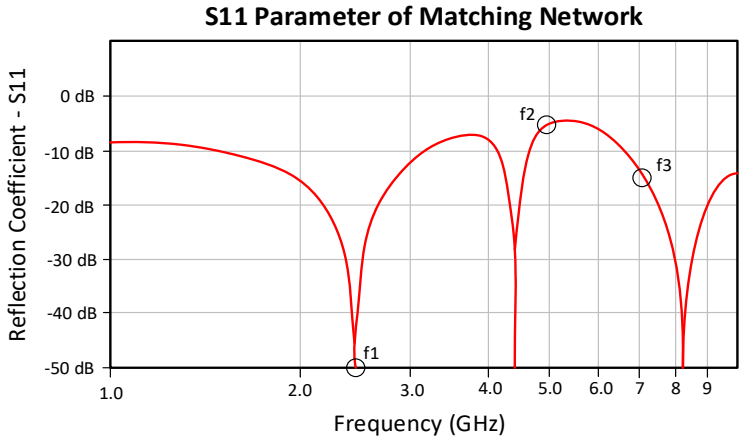

Fig. 4.15: Input port voltage reflection coefficient for RF matching network

4.3.8 Planar Inverted-F Antenna

A Planar Inverted-F Antenna (IFA) was implemented in this design for its compact size, low cost, and high performance [31]. The structure of the PCB patch antenna has an intermittent feed point, rather than at the base. The impedance seen at the system is dependent on the path length back to ground, since it is effectively acting as a short stub on a transmission line [32]. Thus, the system impedance of the antenna can be adjusted by the location of this feed point as seen in Fig. 4.16.

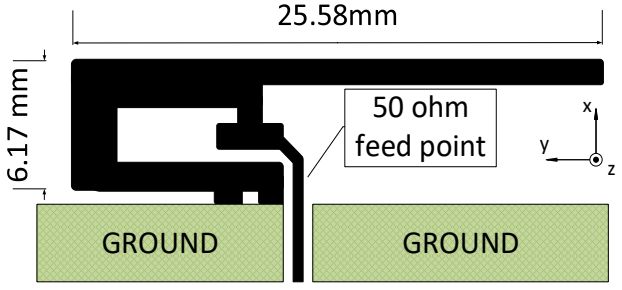

Fig. 4.16: P-IFA dimensions

This is a typical layout for 2.4GHz wireless systems and has been heavily optimized into an industry standard design. Table 4.2 contains maximum measured gains, and reflection measurements from an application note published by Texas Instruments [31].

Table 4.2: Summary of P-IFA properties [31]

Gain in XY plane	1.1 dBi
Gain in XZ plane	3.3 dBi
Gain in YZ plane	1.6 dBi
Reflection	<-15dB
Antenna size	25.7 x 7.5 mm

The application note also provides a measurement of the reflection at the feed point of the antenna (Fig. 4.17). The reflection coefficient is between -17.5 and -25 dB over the Bluetooth bandwidth (2.4-2.5 GHz). Since it is not flat over this range, the resulting power spectrum will vary from 86% to 94%. This corresponds to a 0.6 - 1.3 dBm loss due to reflection. This does not account for other losses or gains within the system.

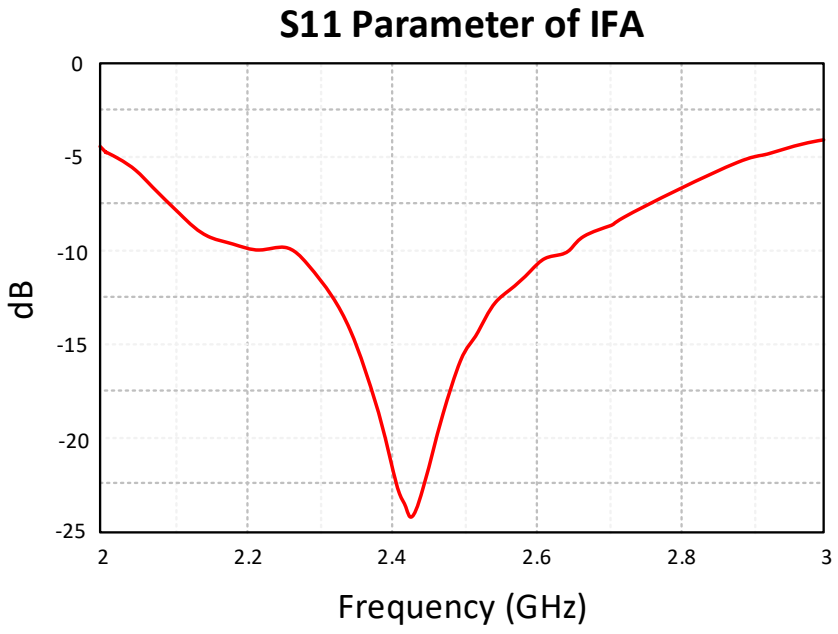

Fig. 4.17: Measured reflection at feed point of antenna [31].

4.4 RF Performance and Adjustments

The design was fabricated and assembled by a board-house based in China. The matching network is very sensitive to component parasitics and must use 0402 sized components which require machine placement and wave soldering. To limit spurious emissions radiated by the system, the PA was placed in an RF blocking cage. Fig. 4.18 shows the physical board layout of the RF front-end.

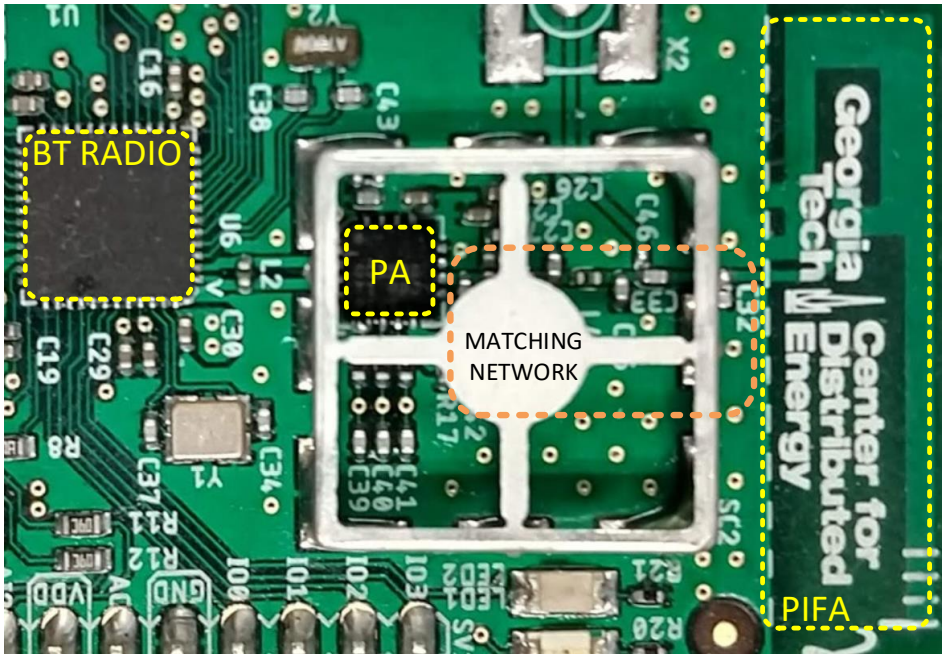

Fig. 4.18: PCB implementation of radio, power amplifier, matching network, and patch antenna.

4.4.1 Testbed Set-Up

The quality of the RF system was tested using the CBT Bluetooth Tester from Rhode and Schwarz. The CBT can perform power, modulation, frequency and bit error rate (BER) tests, as well as spectrum measurements on an active Bluetooth connection without requiring an external spectrum analyzer. The test-bed configuration is detailed in Fig. 4.19.

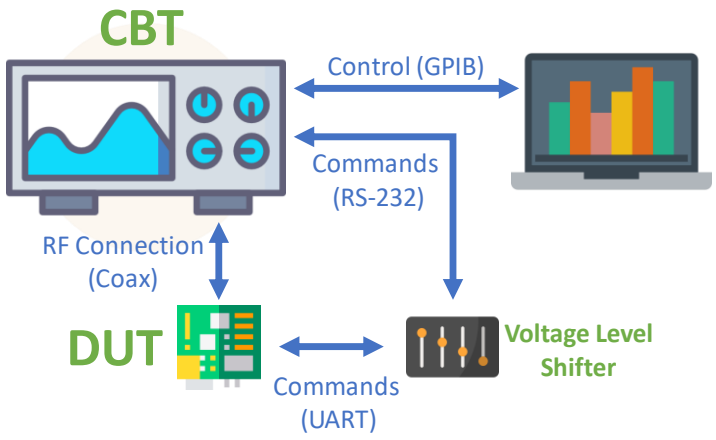

Fig. 4.19: Bluetooth testing configuration

Test commands issued by the CBT are carried over RS-232 at 5V and require a voltage level shifter to communicate with the Device Under Test (DUT) via UART pins. The DUT is then connected directly to the CBT via a coax cable or is placed in shielded box with an internal antenna and coax output. Individual tests can be carried out locally or automated via a computer with GPIB capabilities.

4.4.2 Initial Results: In-Band Emissions

The Kernel design passed 271 of the 277 Bluetooth tests conducted on the first prototype run. While many of the values measured were at the cusp of acceptable ranges, the passing results were better than expected; ostensibly indicating that only minor changes would be required. Where the design failed, however, was in the in-band emissions test. This test measures total power radiated across the spectrum while transmitting on three different channels. A power level mask sets maximum thresholds for a given frequency measured. The first prototype had six frequency bands that violated the emissions mask (Fig. 4.20).

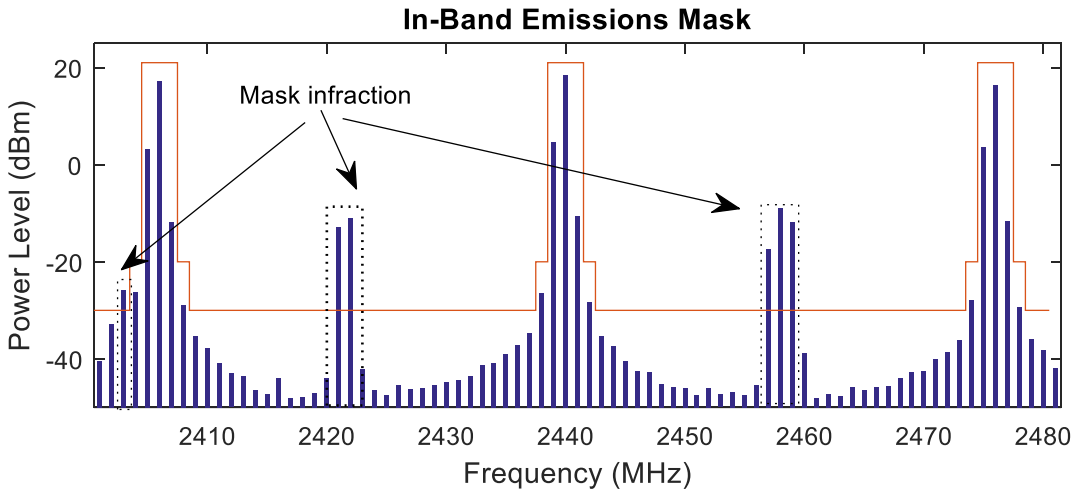

Fig. 4.20: In-band emissions test for Revision A

After examining production Gerber files used by the board house, it was discovered that their isolation requirements for the thermal pads had caused gaps to form along the transmission line (Fig. 4.21). These gaps produced asymmetries along the waveguide and impacted stability. The isolation requirements also limited trace contact to the grounding pad of the PA.

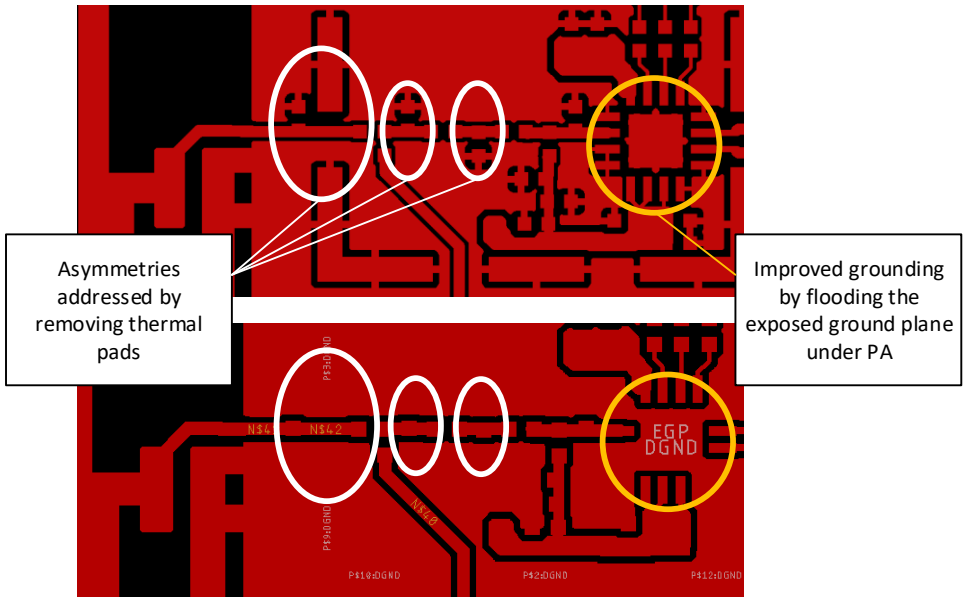

Fig. 4.21: PCB layout changed to address in-band emissions

During transmission, the PA takes 120 mA at 3.3V. In terms of normal Bluetooth signaling, this is the highest power allowed. However, in terms of thermal considerations 400mW is very low power. As a result, the thermal relief was removed from this section of the board to allow for more consistent copper along the transmission lines and grounding pads. A second spin of the board was fabricated and assembled with these layout changes. The layout changes removed the unwanted spurs in subsequent testing (Fig. 4.22). Carrier frequency was also improved; note that the three channels appear more symmetric around their center frequencies.

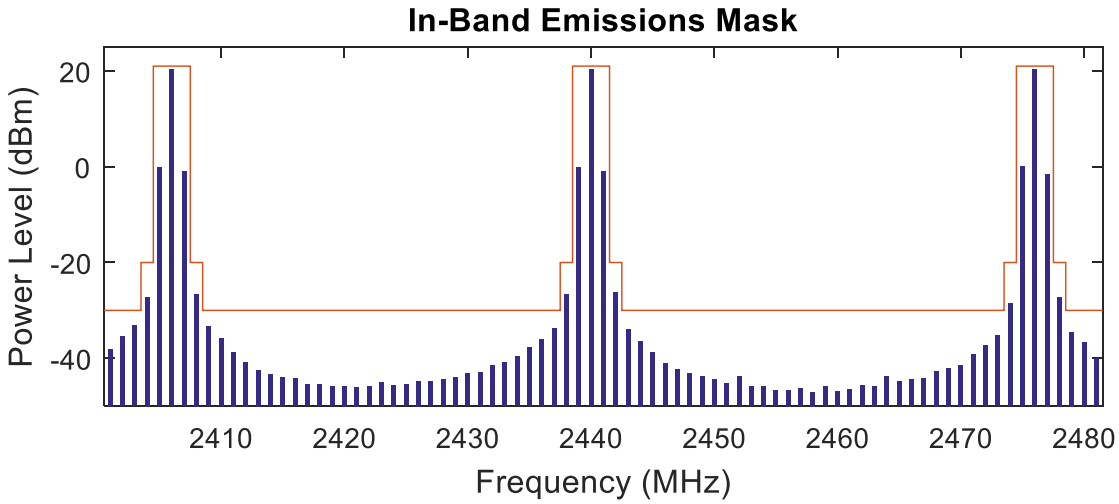

Fig. 4.22: In-band emissions for Revision B

4.4.3 Bluetooth Compliance Testing

With the revisions made, all tests performed were within acceptable ranges. The modified layout not only addressed in-band emissions issues, but also improved values in every test category. Revision B had an output power range of 19.73-20.49 dBm, completely clearing the upper bound of the previous revision, 18.38 dBm (Table 4.3). Packet error

rates were already very good at around 0.07-1.4%, but nearly all test conditions converged on 0% for 1500 packets (Table 4.4).

Table 4.3: Output power

Test Name and Condition	Upper Limit	Revision A	**Revision B**
Average Power Ch. 0	21.1 dBm	17.73 dBm	**20.56 dBm**
Difference (Peak – Avg)	3.0 dB	1.47 dB	**0.45 dB**
Average Power Ch. 19	21.1 dBm	18.38 dBm	**20.42 dBm**
Difference (Peak – Avg)	3.0 dB	0.66 dB	**0.45 dB**
Average Power Ch. 39	21.1 dBm	17.16 dBm	**19.73 dBm**
Difference (Peak – Avg)	3.0 dB	0.62 dB	**0.46 dB**

Table 4.4: Receiver sensitivity for 1500 packets

	Test Name and Condition	Upper Limit	Revision A	**Revision B**
-70 dBm Input	PER Ch.0	30.80%	0.07 %	**0.00 %**
	PER Ch.19	30.80%	0.00 %	**0.00 %**
	PER Ch. 39	30.80%	0.07 %	**0.07 %**
-10 dBm Input	PER Ch.0	30.80%	0.67 %	**0.00 %**
	PER Ch.19	30.80%	1.40 %	**0.00 %**
	PER Ch. 39	30.80%	0.00 %	**0.00 %**

Frequency accuracy, offset, and drift weren't improved by the modified transmission line, but rather the removal of the loading capacitors for the crystal oscillator. The selected 25 MHz oscillator required 9pF of added capacitance at the terminals, however it is likely that the PCB was providing this amount through parasitic effects. The oscillator became more stable upon removal of the capacitors (Table 4.5).

Table 4.5: Carrier frequency offset and drift

Test Name and Condition	Lower	Upper	Loading	**No Loading**
Frequency Accuracy	-150 kHz	150 kHz	-126.39 kHz	**-7.03 kHz**
Frequency Offset	-150 kHz	150 kHz	-128.49 kHz	**-11.05 kHz**
Frequency Drift	-50 kHz	50 kHz	9.91 kHz	**7.15 kHz**
Maximum Drift Rage	-20 kHz	20 kHz	11.94 kHz	**-6.48 kHz**
Initial Frequency Drift	-20 kHz	20 kHz	5.83 kHz	**-4.12 kHz**

4.4.4 Bluetooth Range - Field Test

The Kernels were taken to Piedmont Park in Atlanta, Georgia to conduct a range test. There is a section of the park that contains a large, open, and flat field that spans roughly 400 meters across (Fig. 4.23). This area was chosen as it could approximate the most ideal line of sight scenario, free from elevation changes, obstructions, reflections from nearby buildings, and would have less interference from other wireless systems (namely Wi-Fi).

Fig. 4.23: Open field in Piedmont Park, with location of measured data marked.[3]

The test was conducted by placing the kernel in a fixed location and using a smart phone to connect to the device at various locations. Both the phone app and Kernel provided RSSI outputs to verify when connection and disconnect events occurred. The range tests were all conducted with the same phone as earlier, an LG Nexus 5X, to ensure that the phone's link budget would not vary the results.

As expected, the updated hardware with the Bluetooth range extender performed better than the tests conducted earlier with the Smart Meter. There was, however, an

[3] Map and location data courtesy of Google Maps (maps.google.com)

emerging property that did not appear in earlier tests. During testing, it became clear that there was a discrepancy between the maximum range that a phone could connect to the Bluetooth device, and the range at which the device was able maintain this bond before disconnecting. In the Rev A. test, this discrepancy was over 100 meters difference (Table 4.6). Like in previous RF tests, Rev. B improved considerably upon the performance of the previous revision.

Table 4.6: Range comparison across designs

	Smart Meter	Kernel (Rev. A)	**Kernel (Rev. B)**
Max Connection Range	95m	140m	**225m**
Max Disconnect Range	95m	248m	**320m**

The cause of the two ranges is the Bluetooth protocol's implementation fast-ARQ (Fig. 4.24), similar to stop-and-wait ARQ. During the initial pairing process and key exchange, the Bluetooth protocol is extremely sensitive to dropped packets before disconnection [33]. After connection however, the Bluetooth protocol will be more tolerant to missing packets, and retransmission requests (nACK). Unfortunately, this is fixed into the protocol and cannot be changed through firmware or hardware modifications.

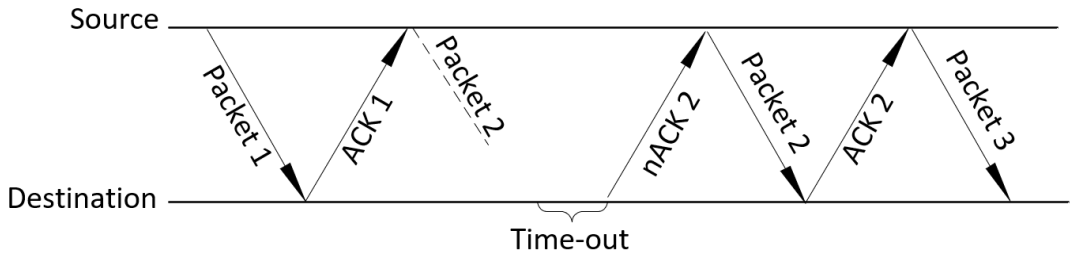

Fig. 4.24: Timing diagram for fast-ARQ

CHAPTER 5

APPLICATION SPECIFIC PROTOTYPING

This chapter details how the GAMMA Kernel can be implemented to fit various applications. It will go into detail on one specific application, a mains voltage monitor, and pose further potential applications and how they could be implemented.

5.1 The Application Board

While the Kernel has a lot of utility and potential, it is unable to function on its own. It ultimately requires external power, and peripheral circuitry to operate. Any functionality that is unique to the specific task at hand will be placed on a separate board, referred to as an application board. This board will power the Kernel and communicate with it via two rows of header pins as seen below (Fig. 5.1).

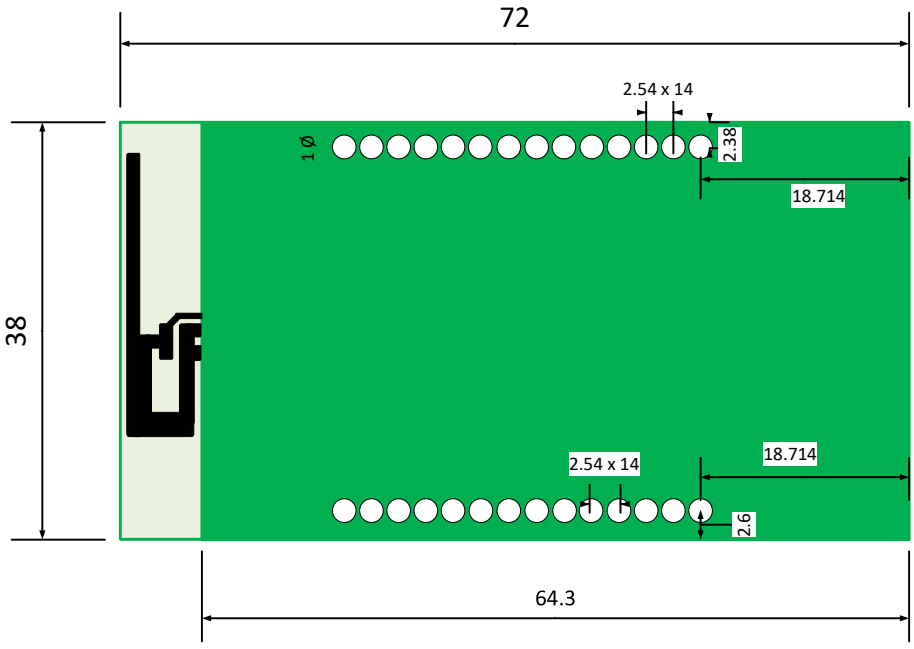

Fig. 5.1: Kernel PCB footprint. All units in mm.

The application board will presumably have functionality without the presence Kernel, but this won't be the case for every application. For some wireless only applications, the secondary board might exclusively be a power interface.

5.2 Mains Voltage - Plug-in Sensor

The first application board designed for the Kernel was a plug-in sensor which monitored mains voltage at a wall-outlet (Fig. 5.2). The power supply was designed to support three phases of 120 V_{AC} or a single phase of 240V_{AC} which would be wired into two split phases with 120 and -120$V_{AC.}$

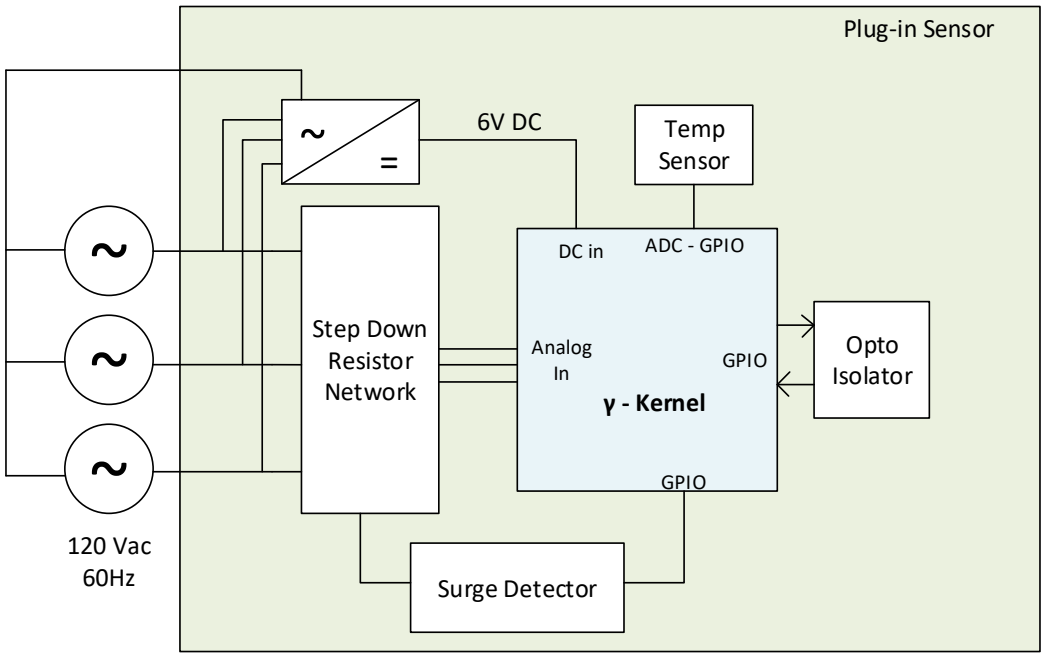

Fig. 5.2: Plug-in sensor interface with Kernel

The device is powered through a three phase AC to DC converter, so that the Kernel can be powered regardless of how the external AC source is configured. The three voltage

inputs are connected to a resistor network which steps down the AC voltage. It also applies a DC bias to ensure that the signal is always positive and can be sampled by the Kernel's on-board ADCs. The three sampled voltages are also connected to a comparator which triggers if the input voltage goes above 10% of the nominal voltage, or $132V_{AC}$. An on-board thermo-diode produces a voltage linearly related to the ambient temperature, allowing for an extra parameter to be sampled and monitored. Lastly, there are two GPIOs from the Kernel which are connected to each other via an optocoupler on the application board. This allows the Kernel to verify connectivity with the application board by sending a signal on one of the GPIOs and receiving it on the other. For visual verification, the opto-coupler is also wired in parallel with an LED.

The plug-in sensor serves three main purposes: to implement a voltage sensor without the need of a dedicated AFE, to act as a test-bed to verify Kernel functionality, and to serve as a deployable GAMMA product to test the network.

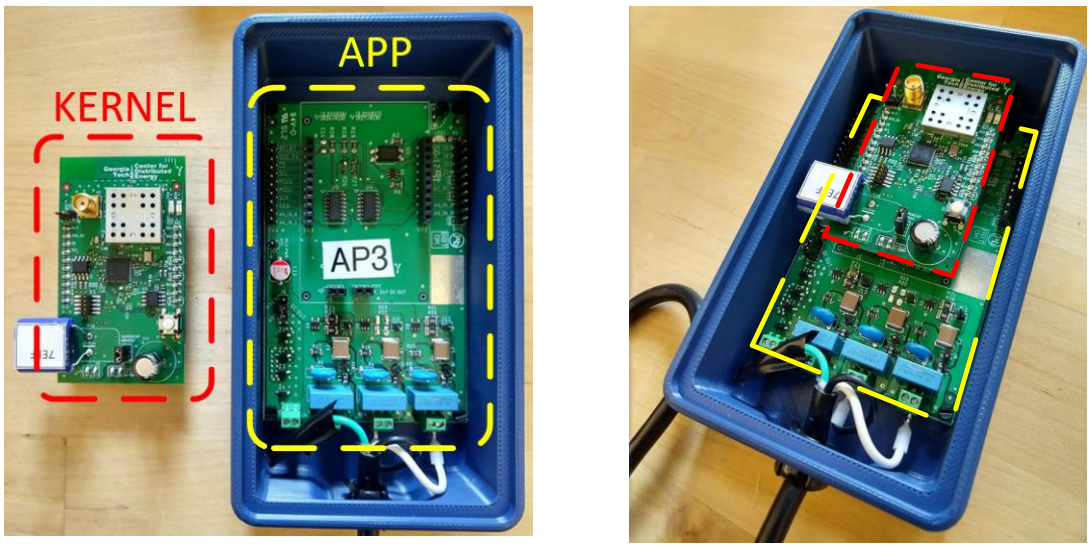

(a) (b)

Fig. 5.3: (a) Kernel and application board. (b) Application board with docked Kernel

5.2.1 Metering

The plug-in sensor records RMS and frequency values for 166ms, or 10 cycles per 1 second interval. These measurements are then averaged into a singular data point, which is rolled into a total average over a 1-minute interval. Upon uplink to the mule app, this is further averaged into 15-minute data points. If more granular data is required, the server can issue a request over a specified period. Additionally, this data is used to generate power events such as surges, swells, sags, frequency deviation, and outages. The on-board temperature sensor will also generate events for over temperature conditions within the enclosure.

The hardware specifications for the plug-in sensor are detailed bellow in Table 5.1. A voltage resolution of 500mV was achieved, like that of the Smart Utility Meter. However, it was slightly less accurate at 0.8%. The plug-in sensor cannot measure current, so no further power measurements were able to be monitored.

Table 5.1: Voltage quality meter specifications

Parameter	Value
Form Factor	13 cm x 7.5 cm x 3.5 cm
Input Range	120 V_{RMS} 60Hz, 240 V_{RMS} 50Hz
Voltage Resolution	500mV
Voltage Accuracy	±0.8%
Temperature Resolution	0.5°C
Temperature Accuracy	±1°C
Sampling Rate	2 kHz
ADC Word Length	12 bits
Flash Memory	32Mb
Bluetooth Range (LoS)	320 m

5.2.2 Platform Performance

To evaluate platform performance, five devices were deployed around campus and the greater Atlanta area. The devices ran for 21 days, and data was collected over this time. To calculate latency, the interval between transmissions were averaged over the total amount of sampled taken:

$$\overline{T_L} = \frac{1}{k}\sum_{n=1}^{k} |T_S - T_D|_n \tag{31}$$

Where $\boldsymbol{k}$, is the total number of samples, $\boldsymbol{T_D}$ is the time stamp when the data was generated on the end-node, and $\boldsymbol{T_S}$ is when it was received on the server end. The platform performance results are listed below in Table 5.2.

Table 5.2: Platform performance summary

Parameter	Value
Total Time	21 Days
Total Data Uploaded	1.77 MB
Min. Latency	1 sec.
Max. Latency	122 hrs.
Avg. Latency	244.5 sec.
Events Recorded	6
Avg. no. of connections / day	12.7
Avg. no. of connections / app / day	9.9
Avg. no. of apps connected to device	2

Several of the devices had reliable and frequent access to data-mules. For these devices, the delay-tolerant network was effectively an on-demand network while the mule was present. These were typically in locations in an office where a worker had the app on their phone, or in a residence where the inhabitant also had the app installed. The devices

deployed in specific labs or conference rooms had delays up five days but were still able to communicate with the server on a weekly basis.

The data collected in this trial was processed on the cloud side and if certain qualifications and permissions were met by the user, displayed on the app. The app would display when the end-node was last synced, as well as voltage, temperature, and frequency measurements over time. Additionally, events such as voltage surge, swells, frequency deviation, and outage would also be displayed on the same screen (Fig. 5.4).

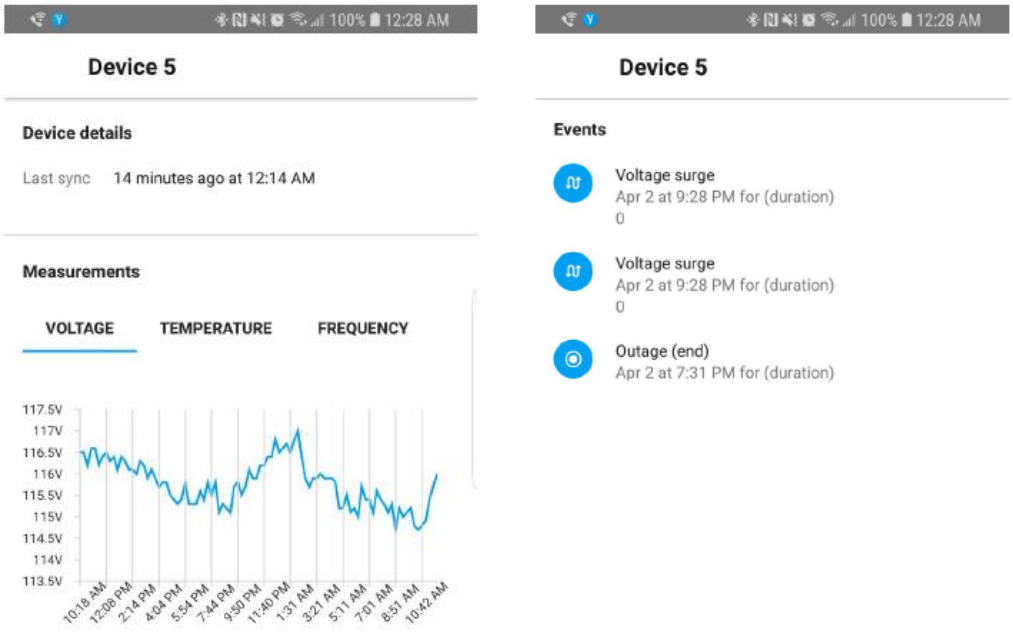

Fig. 5.4: Application interface detailing: last sync, voltage measurement over a set window, and recorded events.

5.3 Potential Applications

The plug-in sensor is only one of many potential devices that can be interfaced with the Kernel to become GAMMA enabled. The Kernel could also be outfitted to serve various networking features within a larger network.

Remote Terminal Unit:

If a fleet manager had multiple devices within a mesh, one dedicated Kernel could be set up to act as a Remote Terminal Unit (RTU), which would collect data from the various end-nodes. The data-mule would then only need to connect to one device to receive and transmit data to the mesh network. The RTU's location could be optimized to increase range and communication efficiency for all devices within the network. That way, end-nodes in harder to reach areas might maintain a more reliable connection pathway to the remote server.

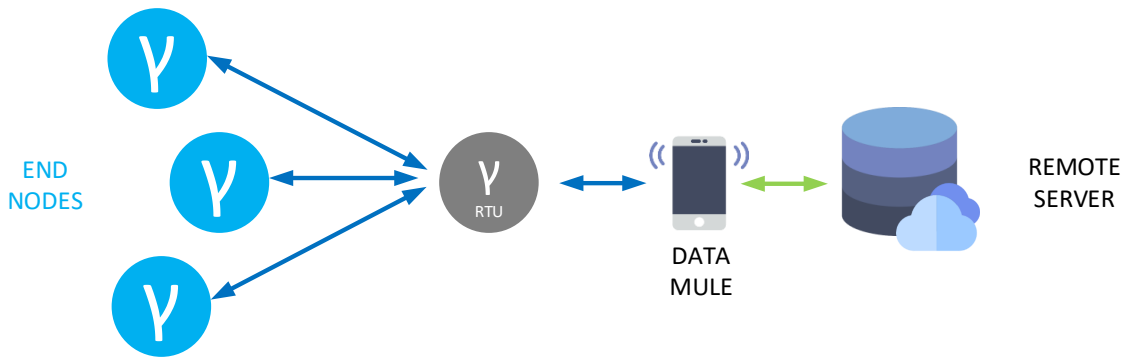

Fig. 5.5: Specialized Kernel to act as RTU

Bluetooth Repeater:

While a BLE range of 300m is impressive in comparison to most consumer end products, this range is largely being limited by the output power available by the smart phone. If two Kernels with identical link budgets are used, the range could potentially be increased to over a kilometer; significantly further than with the smart phone. The Bluetooth MCU used on the kernel can sustain up to two simultaneous connections. If configured with specialized firmware, a Kernel could be set up to act as a range extender or relay for a smart phone. In this scenario an application board would likely be a small

battery, with some power management circuitry. If packaged small enough, the relay could be carried on a person or mounted on a vehicle. This would increase the range of the data-mule from 300 meters to over a kilometer line-of-sight.

Fig. 5.6: Kernel configured to act as a Bluetooth relay / range extender.

Streamlined Smart Utility Meter:

The smart utility meter, covered earlier, could also be retrofitted to be Kernel compliant. This would likely make the board smaller over-all, as components and routing could be implemented underneath the Kernel. The total height will increase a few millimeters, as the relays on the board are nearly 30mm on their own. Special attention would need to be paid to the interconnection of the Kernel and the application board, as the AFE will only tolerate up to 25mV of common mode noise.

Other Possible Applications:

With a flexible design scheme, there are numerous applications that could be implemented: solar irradiance monitoring, air quality meter, soil pH regulator, bridge displacement monitoring, stick-on transformer sensor, and many more.

CHAPTER 6

ON-DEMAND RADIO EXPANSION

The network capabilities of the end-device can be further diversified by incorporating a dedicated radio into the system. This chapter details a version of the core-design that has been expanded to include a GSM modem.

6.1 Application-specific Implementation

The design flexibility of the Kernel allows for multiple ways to expand the network structure of the end-node. For systems that already have dedicated radios available, these can be interfaced directly with the Kernel via the available GPIO pins. If a new radio is desired, this can be handled via an application board which will interface with the Kernel. However, for designs that do not currently have wireless communications or resources to design such an application board, a specialized version of the Kernel with a dedicated radio was created to address this use-case.

6.2 Architecture Overview

The fundamental structure of the Kernel remains largely the same for the upgraded design, referred to as the Kernel Plus. New modifications include an on-board dedicated GSM module, a secondary MCU to operate the module, and an upgraded power supply to handle the current load required by the additional circuitry. A block diagram for the expended Kernel design can be found in Fig. 6.1.

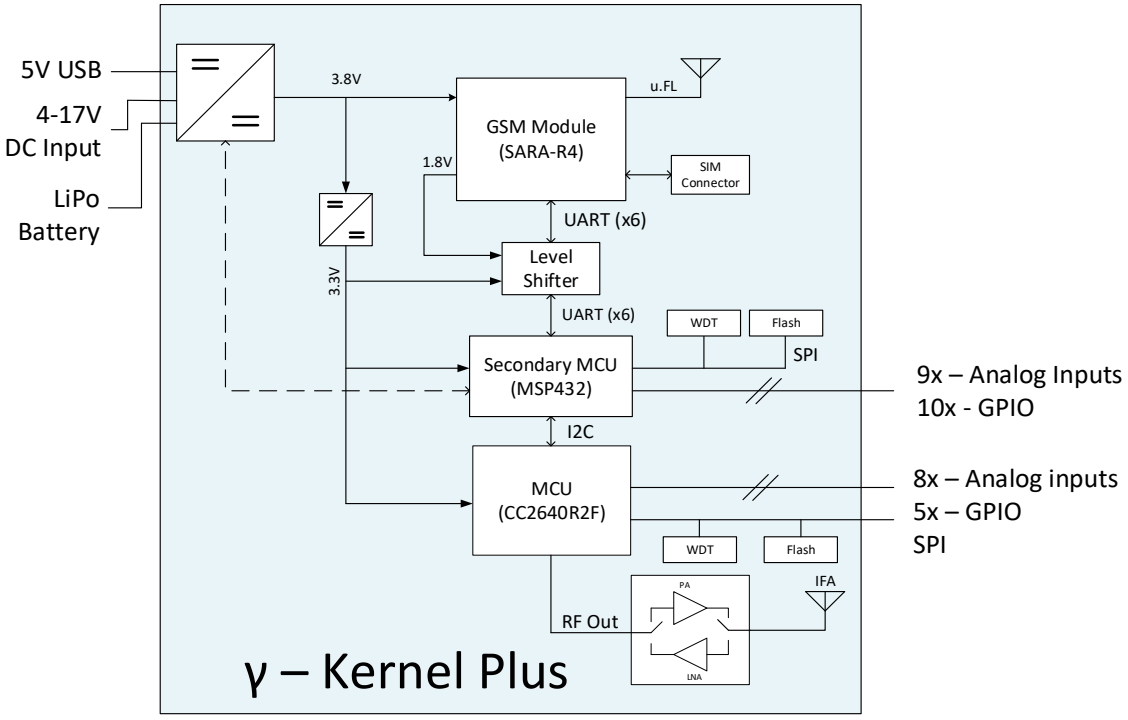

Fig. 6.1: Block diagram for Kernel Plus, a GSM enabled GAMMA device.

6.3 On-Demand Radio

The addition of GSM module predicated most of the design considerations when expanding the base-Kernel. These were the redesign of the power supply, the inclusions of the secondary MCU, and provisions for a rechargeable battery.

6.3.1 Voltage Rails

The GSM module requires a 3.8V power supply and must be able to support surge currents of up to 2 amps. This is beyond the supply capability of the LDO used in the base-Kernel and needed to be refitted with a switch mode power supply (SMPS) and external inductor. The output of the SMPS goes directly to the GSM module and a secondary SMPS which steps 3.8V down to 3.3V used by the rest of the system. The input and outputs of

the GSM module are also on a 1.8V rail. The module provides a local 1.8V source, which is used to operate a level shifting IC to interface with 3.3V communications.

6.3.2 Outage Contingency

The increased power budget also negates the utility of the super-capacitor, as it would get depleted in a matter of seconds. In lieu of a capacitor, the main SMPS has a built-in charging circuit for a 3.7V LiPo battery. This can dramatically increase the autonomy of the system during a power outage but will ultimately decrease the longevity of the system once the battery needs to be replaced.

6.3.3 Additional MCU

The interface to the GSM module requires 3-4 UART lanes, depending on the flow-control requirements of the system. Since the Bluetooth MCU on the Kernel can only support 1 UART channel, an additional MCU with additional UART capabilities is required. The two MCUs are connected to one-another via I2C. The external I2C connection of the Kernel has been replaced by one on the secondary MCU to remain pin-compatible.

6.4 Form Factor

The form factor of the Kernel-plus is essentially double that of the base-Kernel. The length of the board has remained the same, but the width has increased by a factor of two. The additional I/O pins on the secondary MCU are available through additional header pins located in the middle and ends of the board, mirroring the footprint of the base-Kernel.

Unfortunately, physical prototypes were not available in time for testing and verification. However, a rendering of the PCB layout is available in Fig. 6.2, to show the expanded form-factor and functional blocks.

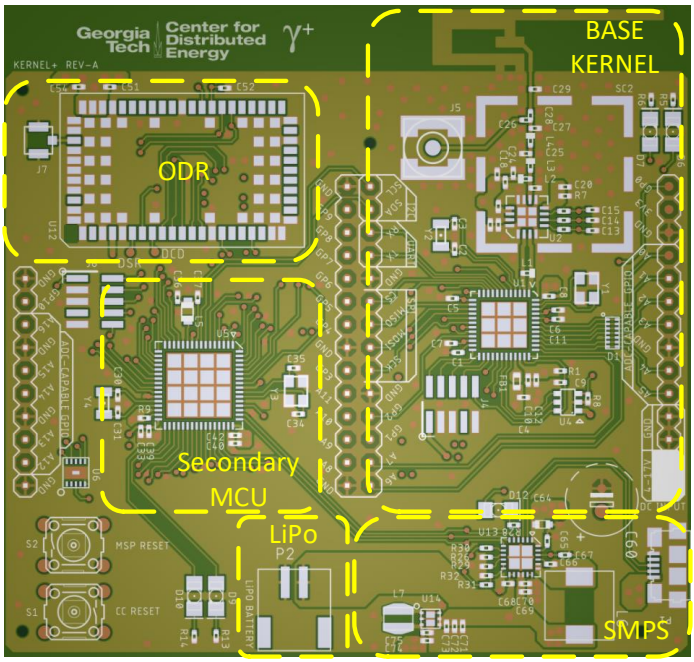

Fig. 6.2: PCB layout of Kernel-plus with functional blocks highlighted.

6.5 Future Work

As stated previously, prototypes were not available in time for evaluation, design debugging, and performance testing. Likewise, the impact on system performance cannot be quantified. However, the schematics and layout for the upgraded board have been designed, and the foundation for future work in this space have been established. Like with the Kernel, an application board will be required to act as a test bed for functionality verification. Since this requires support for an additional MCU, and ODR extensive software development will be required before further hardware development can take place.

CHAPTER 7

CONCLUSIONS AND FUTURE WORK

This research serves as both a proof of concept for the GAMMA platform, as well as a reference point for subsequent designs. Despite considerable progress on hardware, firmware, and software the platform remains in a fledgling state. The foundation has been laid, but still has room for improvements and developments as new challenges arise. This chapter discusses current limitations, and future work that can build upon the research presented in this thesis.

7.1 Discussion and Future Work

7.1.1 Scalability and Economic Analysis

The hardware detailed in this paper was designed in low-volumes and using parts that were readily available for the chosen manufacturers. This is acceptable for prototyping but must be revaluated for larger production. This could possibly involve something as innocuous as swapping out less expensive and pin-compatible components but might require minor design adjustments if new ICs are required to drive cost down. Scalability for this design must simultaneously take economic factors into account without compromising performance. An in-depth economic analysis of the system at full-scale production will be required to fully demonstrate the value of GAMMA and validate the business-case.

7.1.2 Network Functionality

The functionality of the DTN hinges on the presence of data-mules. It is currently unclear what population size of participants is necessary to ensure network functionality, and stability. The existence and presence of data-mules is also dependent of willing participants, who will need incentivization to download this app. Since this app will use power and data from the user, the incentivization will likely need to be economical. The user will also be required to have Bluetooth and GPS always on. Some degree of social engineering will be required to convince the user to not turn these radios off.

7.1.3 Kernel-compliant Smart Utility Meters

Since the smart utility meter was designed prior to the conception of the Kernel, it does not have provisions for the pluggable hardware. Future work could involve revising this design to make the smart utility meter an application board for the Kernel and or Kernel-plus. Since the AFE has stringent noise requirements, extra care must be taken that the interconnects of the design do not cause the system to fail. The work in this space could be coupled with the interconnect redesign and serve as a test-structure.

7.1.4 Board-to-board Interconnects

The GAMMA Kernel, and Kernel-plus can be improved by designing a more space effective interconnect. The current interconnects are header pins which mate with a socket on the application board. While this does allow for components and routing under the Kernel and above the application board, this sets a height minimum of 2.5 cm, which might be bulky for certain applications. Another approach to this problem could be a redesign

utilizing only one side for components. This would allow for LGA style pads, or castellated-vias to interconnect with the application board.

7.1.5 IEEE Empower a Billion Lives

Plans are currently in the works to open the GAMMA platform and Kernel hardware for use in the IEEE competition empower a billion lives. This competition focuses on fostering innovative solutions to address energy poverty around the globe. Solutions presented in the competition are expected to be holistic, regionally relevant, scalable, and leverage modern technologies at declining prices.

7.2 Conclusions

In this work, I presented a scalable solution for the communication needs of asset monitoring via a Bluetooth platform called GAMMA. GAMMA can be rapidly and easily incorporated into new or existing systems by interfacing with a feature rich module, the GAMMA Kernel, which offloads much of the design and development time. While certainly not without its own short comings, this study demonstrates that the flexibility offered by the platform can provide access to the cloud for low-cost applications that might otherwise be overlooked.

REFERENCES

[1] R. Morello, C. De Capua, G. Fulco and S. C. Mukhopadhyay, "A Smart Power Meter to Monitor Energy Flow in Smart Grids: The Role of Advanced Sensing and IoT in the Electric Grid of the Future," *IEEE Sensors Journal,* vol. 17, no. 23, pp. 7828-7837, Dec.1, 1 2017.

[2] M. McGranaghan and B. Deaver, "Sensors and monitoring challenges in the smart grid," in *2012 Future of Instrumentation International Workshop (FIIW) Proceedings*, Gatlinburg, TN, 2012, pp. 1-4.

[3] J. McDonald, *Recent Trends in Substation Automation and Enterprise Data, IEEE Educational Course,* [Online] http://ieeexplore.ieee.org/servlet/opac?mdnumber=EW1161.

[4] J. Taft and P. De Martini, "PNNL-25249 'Sensing and Measurement Architecture for Grid Modernization'," Pacific Northwest National Laboratory, Richland, 2016.

[5] V. C. Gungor et al, "A survey on communication networks," *Computer Networks Journal,* vol. 50, pp. 877-897, May 2006.

[6] V. C. Gungor et al, "A survey on smart grid potential applications and communication requirements," *IEEE Trans. on Ind. Info,* vol. 9, no. 1, pp. 28-42, Feb. 2013.

[7] W. Wang, Y. Xu and M. Khanna, "A survey on the communication architectures in smart grids," *Computer Networks,* vol. 55, no. 15, pp. 3604-3629, Oct. 2011.

[8] E. Span, L. Niccolini, S. D. Pascoli and G. Iannacconeluca, "Last-meter smart grid embedded in an Internet-of-Things platform," *IEEE Trans. Smart Grid,* vol. 6, no. 1, pp. 468-476, Jan. 2015.

[9] H. G. S. Filho, J. P. Filho and V. L. Moreli, "The adequacy of LoRaWAN on smart grids: A comparison with RF mesh technology," in *2016 IEEE International Smart Cities Conference*, Trento, pp. 1-6, 2016.

[10] Y. Sun, H. Song, A. J. Jara and R. Bie, "Internet of Things and big data analytics for smart and connected communities," *IEEE Access,* vol. 4, pp. 766-773, 2016.

[11] A. Rahmah, T. Nakanishi and A. Fukuda, "Delay tolerant network for developing countries," in *2013 International Conference on Informatics, Electronics and Vision*, Dhaka, pp. 1-6, 2013.

[12] A. Galati, T. Bourchas, S. Siby, S. Frey, M. Olivares and S. Mangold, "Mobile-enabled delay tolerant networking in rural developing regions," in *IEEE Global Humanitarian Technology Conference*, San Jose, pp. 699-705, 2014.

[13] H. Ntareme, M. Zenna and B. Pehrson, "Delay tolerant network on smartphones," in *ACN ExtremeCom*, Galapagos Islands, Ecuador, 2011.

[14] "Phone, Tablet & PC | Bluetooth Technology Website," Bluetooth Special Interest Group., [Online]. Available: https://www.bluetooth.com/markets/phone-pc. [Accessed 16 June 2018].

[15] Bluetooth Special Interest Group, "Bluetooth Core Specification 4.2 - FAQ," 12 2014. [Online]. Available: http://www.ineltek.com/wp-content/uploads/2015/09/20160330-Bluetooth4-2FAQ.pdf. [Accessed 5 June 2018].

[16] Q. Cetina, R. Roscoe and P. Wright, "Challenges for smart electricity meters due to dynamic power quality conditions of the grid: A Review," in *IEEE Intl. Workshop on Applied Measurements for Power*, Liverpool, Sept. 2017.

[17] L. Alejandro et al, "Global market for smart electricity meters: Government policies driving strong growth," in *Office of Industries, U.S. International Trade Commission*, No. ID-013, June 2014.

[18] R. Pillai, R. Bhatnagar and H. Thukral, "AMI rollout strategy and costbenefit analysis for India," in *Proc. Intl. Conf. Sustainable Green Buildings & Communities*, Chennai, Dec. 2016.

[19] N. Andrei et al, "Smart metering platform as a solution for data analysis," in *Proc. Intl. Conf. Energy & Env*, Romania, Oct. 2017.

[20] J. Peppanen et al, "Distribution system low-voltage circuit topology estimation using smart metering data," in *Proc. IEEE PES T&D Conf. & Expo*, 2016.

[21] T. Velayudham, R. Ganesh and R. Kanimozhi, "Locating ground fault in distribution systems using smart meter," in *Proc. Intl. Conf. Electronics Communication Aerospace Technology*, Coimbatore, April 2017.

[22] A. Munoz and J. Rosa, "Integrating power quality to automated meter reading," *IEEE Ind. Electron. Mag.*, vol. 2, no. 2, p. 1018, 2008.

[23] S. Depuru et al, "Smart meters for power grid— Challenges, issues, advantages and status," in *Proc. IEEE PES Power Sys. Conf. Exp.*, Pheonix, Mar. 2011.

[24] T. R. Kuphaldt, "Chapter 14 - Transmission Lines," in *Lessons in Electric Circuits - Vol. II Alternating Current*, EETech Media, LLC..

[25] B. C. Wadell, "Coplanar Waveguide with Ground," in *Transmission Line Design Handbook*, Norwood, MA, Artech House, Inc., 1991, pp. 79-80.

[26] MathWorks, "Complete elliptic integrals of first and second kind," [Online]. Available: https://www.mathworks.com/help/matlab/ref/ellipke.html. [Accessed 23 June 2018].

[27] Bittele Electronics Inc., "Standard Multi-layer PCB Stackup," 2012. [Online]. Available: https://www.7pcb.com/Upload_file/Multi-layer-stack-up.pdf. [Accessed 3 July 2018].

[28] Institute of Printed Circuits, *6012B - Qualification and Performance Specification for Rigid Printed Boards*, Northbrook, Illinois, August 2004.

[29] Bittele Electronics Inc., "PCB Fabrication Capabilities," [Online]. Available: https://www.7pcb.com/PCB-Fabrication.php. [Accessed 3 July 2018].

[30] W. L. Stutzman and G. Thiele, in *Antenna Theory and Design*, Antenna Theory and Design, 2012, p. 177.

[31] Texas Instruments, *Application Report - SWRU120C - 2.4-GHz Inverted F Antenna*, Februrary 2017.

[32] P. S. Hall, E. Lee and C. T. P. Song, "Planar inverted-F antennas," in *Printed Antennas for Wireless Communications*, John Wiley & Sons, 2008, pp. 192-227.

[33] R. Kai, "Bluetooth Pairing Part 1 Pairing Feature Exchange | Bluetooth Technology Website," Bluetooth Special Interest Group, 29 3 2016. [Online]. Available: https://blog.bluetooth.com/bluetooth-pairing-part-1-pairing-feature-exchange. [Accessed 27 June 2018].